Microbial reduction of iron(III)-rich nontronite and uranium(VI)

Gengxin Zhang[1], John M. Senko[1], Shelly D. Kelly[2], Hui Tan[1], Kenneth M. Kemner[2] and William D. Burgos[1*]

[1]Department of Civil and Environmental Engineering, The Pennsylvania State University, University Park, PA, [2]Biosciences Division, Argonne National Laboratory, Argonne, IL.

Prepared for re-submission to: *Geochimica Cosmochimica Acta*

Title running head: bioreduction of nontronite and uranium

*Corresponding author: William D. Burgos, Dept. of Civil and Environmental Engineering, The Pennsylvania State University, 212 Sackett Building, University Park, PA, 16802-1408, phone: 814-863-0578; fax: 814-863-7304; e-mail: wdb3@psu.edu.

ABSTRACT

To assess the dynamics of microbially mediated U-clay redox reactions, we examined the reduction of iron(III)-rich nontronite NAu-2 and uranium(VI) by *Shewanella oneidensis* MR-1. Bioreduction experiments were conducted with combinations and varied concentrations of MR-1, nontronite, U(VI) and the electron shuttle anthraquinone-2,6-disulfonate (AQDS). Abiotic experiments were conducted to quantify U(VI) sorption to NAu-2, the reduction of U(VI) by chemically-reduced nontronite-Fe(II), and the oxidation of uraninite, $U^{(IV)}O_{2(s)}$, by nontronite-Fe(III). When we incubated *S. oneidensis* MR-1 at lower concentration ($0.5*10^8$ cell mL^{-1}) with nontronite (5.0 g L^{-1}) and U(VI) (1.0 mM), little U(VI) reduction occurred compared to nontronite-free incubations, despite the production of abundant Fe(II). The addition of AQDS to U(VI)- and nontronite-containing incubations enhanced both U(VI) and nontronite-Fe(III) reduction. While U(VI) was completely reduced by *S. oneidensis* MR-1 at higher concentration ($1.0*10^8$ cell mL^{-1}) in the presence of nontronite, increasing concentrations of nontronite led to progressively slower rates of U(VI) reduction. U(VI) enhanced nontronite-Fe(III) reduction and uraninite was oxidized by nontronite-Fe(III), demonstrating that U served as an effective electron shuttle from *S. oneidensis* MR-1 to nontronite-Fe(III). The electron-shuttling activity of U can explain the lack or delay of U(VI) reduction observed in the bulk solution. Little U(VI) reduction was observed in incubations that contained chemically reduced nontronite-Fe(II), suggesting that biologic U(VI) reduction drove U valence cycling in these systems. Under the conditions used in these experiments, we demonstrate that iron-rich smectite may inhibit or delay U(VI) bioreduction.

1. INTRODUCTION

Uranium pollution is a consequence of the nuclear age and is problematic because of its complicated speciation and varied sorption affinity for sediment minerals. Poorly soluble U(IV) minerals and highly soluble U(VI) species govern uranium mobility in groundwater and sediments (Grenthe et al., 1992). Soluble U(VI) species can be biologically or chemically reduced to the sparingly soluble U(IV) mineral uraninite to retard uranium transport. Bacterial reduction of U(VI) to U(IV) may be exploited for *in situ* remediation of contaminated sites (Anderson et al., 2003; Istok et al., 2004; Wu et al., 2006a; Wu et al., 2006b). The low solubility of uraninite and relatively high rates of bacterial U(VI) reduction and its potential cost-effectiveness makes bioremediation an attractive approach for large sites with relatively low levels of contamination (Brooks et al., 2003).

Dissimilatory metal-reducing bacteria (DMRB) gain energy by utilizing a variety of oxidized metals such as Cr(VI), Fe(III), Mn(VI), Tc(VII) and U(VI) as terminal electron acceptors (TEAs) with organic acids, alcohols or H_2 as electron donors (Lovley, 1993; Nealson and Saffarini, 1994). Iron is the fourth most abundant element and the most dominant redox active metal in the Earth's crust. Iron-bearing clay minerals are widely distributed in soils and sediments (Schwertmann and Cornell, 2000), and represent a large mass of electron acceptor Fe(III) for DMRB (Kostka et al., 2002). In subsurface sediments containing U(VI), DMRB may encounter multiple electron acceptors, and when evaluating the potential for *in situ* uranium remediation, it is important to understand how the presence of alternative electron acceptors such as

61 nitrate, Mn(III/IV) oxides, and Fe(III) oxides affect U(VI) remediation (Wielinga et al.,
62 2000).

63 Smectite is a dioctahedral layer phyllosilicate that is ubiquitous in soils and
64 sediments. Structural Fe in smectite often accounts for about half of the Fe pool in soils
65 and sediments (Favre et al., 2006). The Fe(II)/(III) redox couple generally has a higher
66 half-cell reduction potential than the U(IV)/(VI) redox couple (Table 1), such that Fe(III)
67 may be a more thermodynamically favorable TEA than U(VI) (Fredrickson et al., 2000).
68 However, the actual potentials are dependent upon several factors such as mineralogy,
69 speciation, solubility, concentration, and pH. For example, based on reduction potentials,
70 Fe(III) (oxyhydr)oxides may be respired in preference to uranyl carbonate complexes that
71 may in turn be respired in preference to structural Fe(III) in iron-rich smectites.
72 However, bioreduction of soluble U(VI) species may be physiologically easier (and
73 therefore kinetically favored) compared to bioreduction of solid-phase ferric oxides or
74 structural Fe(III) in phyllosilicates. In addition to thermodynamic and kinetic constraints,
75 differences in the mass of Fe(III) (e.g., %-levels) and U (e.g., μM-levels) will exert an
76 effect on TEA utilization. At present, it is difficult to predict the fate of U(VI) as
77 microbial metal reduction proceeds in iron(III)-rich clay-containing sediments.

78 In addition to "direct" microbial reduction of U(VI), the "indirect" abiotic
79 reduction of U(VI) by various reactive forms of Fe(II) (or other reductants) may be an
80 equally important process. Experiments have demonstrated that U(VI) can be reduced by
81 Fe(II) sorbed to a variety of iron oxides (Liger et al., 1999; Fredrickson et al., 2000; Jeon
82 et al., 2004b; Jang et al., 2008), Fe(II)-containing natural sediments (Behrends and Van
83 Cappellen, 2005; Jeon et al., 2005), Fe(II)-containing carboxyl-functionalized

84 microspheres (Boyanov et al., 2007), structural Fe(II) in green rust (O'Loughlin et al.,
85 2003), and structural Fe(II) in magnetite (Missana et al., 2003). Experiments have also
86 demonstrated that structural Fe(II) in specimen and natural smectites can reduce
87 nitroaromatic compounds (Hofstetter et al., 2003; Hofstetter et al., 2006), chlorinated
88 aliphatics (Sorensen et al., 2005), pesticides (Elsner et al., 2004), Cr(VI) (Gan et al.,
89 1996; Taylor et al., 2000), and Tc(VII) (Peretyazhko et al., 2007).
90 The objective of this research was to study the interactions between uranium(VI)
91 and the iron(III)-rich smectite nontronite NAu-2 during their concomitant biological
92 reduction. Bioreduction experiments were designed to measure the effects of variable
93 concentrations of either U(VI) or nontronite-Fe(III) and the presence/absence of the
94 electron shuttling compound anthraquinone disulfonate (AQDS) on the net reduction of
95 all TEAs. Abiotic reduction experiments were conducted to measure the reduction of
96 U(VI) by chemically-reduced nontronite-Fe(II), and the oxidation of biogenic uraninite
97 by unaltered nontronite-Fe(III) to determine the relative importance of other operative
98 redox processes. The sorption of U(VI) to nontronite was measured as a function of pH
99 and ionic strength to quantify the distribution of aqueous and nontronite-sorbed U(VI) in
100 these systems. Wet chemical methods were used to measure reaction kinetics and
101 reaction products were characterized by scanning electron microscopy, X-ray diffraction,
102 and X-ray absorption spectroscopy.

2. EXPERIMENTAL SECTION

2.1. Cell cultivation

Shewanella oneidensis MR-1 (referred to hereafter as MR-1) was cultured in a chemically defined minimal medium (McDonough, 2006; Burgos et al., 2008). MR-1 cells were harvested by centrifugation (15 min and 20 °C at 3,500 g), washed three times with anoxic 30 mM $NaHCO_3$ buffer (pH 6.8, prepared under an 80:20% N_2:CO_2 atm) and resuspended in the same buffer. Cell density was measured by absorbance at 600 nm and correlated to cell number by acridine orange direct counts.

2.2. Mineral preparation

Nontronite NAu-2, an iron-rich variety of smectite from Uley graphite mine, South Australia (Keeling et al., 2000) was purchased from the Source Clays Repository (West Lafayette, IN). The formula for NAu-2 is $M^{+}_{0.72}(Si_{7.55}Al_{0.16}Fe_{0.29})(Al_{0.34}Fe_{3.54}Mg_{0.05})O_{20}(OH)_4$ where M may be Ca, Na or K (Gates et al., 2002). A clay fraction (0.5 – 2.0 μm) was suspended in 1 M NaCl for one week, separated in distilled water by centrifugation, washed repeatedly until no Cl^- was detected by silver nitrate, and then air-dried. This Na-saturated nontronite was pure without any other mineral phases (as determined by XRD) and contained 23.4% total iron (4.2 mmol Fe/g) in its structure with almost all (99.4%) iron as Fe(III) (Keeling et al., 2000). The majority of structural Fe(III) in NAu-2 is contained within octahedral layers (92 % Fe_T) and the remainder in tetrahedral layers (8 % Fe_T) (Gates et al., 2002; Jaisi et al., 2005). The BET surface area of the air-dried nontronite was determined to be 42.5 m^2/g based on N_2 adsorption.

125 **2.3. Uranium – nontronite adsorption experiments**

126 Uranyl nitrate was dissolved in distilled deionized water to produce a stock
127 concentration of 1.0 mM U(VI). Sorption of uranyl onto nontronite was measured as a
128 function of pH at 10 – 14 duplicated pH values (pH 2.5–9.0) and four ionic strengths
129 (0.001, 0.01, 0.1 and 1 M $NaNO_3$). For each batch system (50 mL Teflon centrifuge
130 tubes), uranyl nitrate stock solution was added to achieve an initial concentration of 0.01
131 mM U(VI) that reacted with a final nontronite concentration of 3.0 g L^{-1}. Variable
132 amounts (μL quantities) of 0.01 M HNO_3 or 0.01 M NaOH were added to each tube to
133 give the desired range in equilibrium pH values. All experiments were conducted at
134 room temperature under atmospheric conditions. All tubes (ca. 20 mL suspension, 30 mL
135 air) were equilibrated with atmospheric P_{CO2} through a combination of passive mixing
136 and active purging throughout the 10 – 14 day sorption period. Tubes were mixed by
137 end-over-end rotation (7 rpm) except when periodically placed on a shaker table (80 rpm)
138 with loosened caps. Tubes were also periodically purged with filter-sterilized air during
139 the sorption period. After equilibration, suspensions were centrifuged for 10 min at
140 14,100 g and room temperature. The pH of the supernatant was measured using a
141 combination electrode (Fisher Scientific), and the quantity of U(VI) sorbed was
142 calculated from the difference between initial total and final aqueous U(VI)
143 concentrations (measured by kinetic phosphorescence analysis (KPA) as described
144 below). No loss of U(VI) from solution was measured in nontronite-free controls.
145 Sorption of uranyl onto nontronite was measured as a function of [U(VI)] in
146 anoxic 30 mM $NaHCO_3$ to quantify the distribution of U(VI) in the bioreduction
147 experiments. Sorption was measured in duplicate at 10 initial total U(VI) concentrations

148 ranging from 0.025 mM to 1.5 mM with a constant nontronite concentration of 5.0 g L^{-1}.
149 Serum bottles were equilibrated for ten days (under 80:20% N_2:CO_2 atm), and the
150 quantity of U(VI) sorbed was calculated from the difference between initial total and
151 final aqueous U(VI) concentrations (measured by KPA).

152 **2.4. Bacterial reduction experiments**

153 MR-1 bioreduction experiments were conducted in the presence or absence of
154 U(VI), nontronite or anthraquinone-2,6-disulfonate (AQDS) to examine the effects of
155 multiple electron acceptors on concomitant U(VI) and Fe(III) reduction. Uranyl acetate
156 was dissolved in anoxic 30 mM $NaHCO_3$ to produce a stock concentration of 25 mM
157 U(VI). Speciation modeling using PHREEQC (Parkhurst et al., 1999) confirmed that
158 U(VI) was undersaturated with respect to schoepite ($UO_2(OH)_2 \cdot H_2O$(schoepite) + $2H^+$ =
159 UO_2^{2+} + $3H_2O$; log K = 5.39) for concentrations >25 mM U(VI) in this buffer. Sterile
160 nontronite suspensions (100 g L^{-1}) were prepared in anoxic 30 mM $NaHCO_3$ and served
161 as stock suspensions for subsequent experiments. Nontronite suspensions were sterilized
162 by a five-minute exposure to microwave radiation (Keller et al., 1988), and sterility was
163 confirmed by lack of bacterial growth in tryptic soy broth following a 48 hr aerobic
164 incubation at 30 ^oC. AQDS was dissolved in anoxic 30 mM $NaHCO_3$ to produce a stock
165 concentration of 1.0 mM. Variable amounts of uranyl acetate, nontronite or AQDS stock
166 solutions were added to anoxic 30 mM $NaHCO_3$ in 120 mL glass serum bottles.
167 Nontronite and uranyl acetate were equilibrated for two weeks before inoculation with
168 MR-1. Nontronite concentrations ranged from 0 to 5.0 g L^{-1}, uranyl acetate
169 concentrations ranged from 0 to 1.5 mM, and AQDS concentrations were 0 or 0.10 mM
170 depending on the experiment. MR-1 was inoculated at either $0.5*10^8$ or $1.0*10^8$ cells

171 mL^{-1} (final concentrations) with sodium lactate (5 mM) provided as the electron donor.
172 Cell-free abiotic controls were prepared along with every experiment. All incubations
173 were conducted in anoxic 30 mM $NaHCO_3$ at room temperature in the dark with no
174 mixing except for sample collection. After cells were added, samples were periodically
175 removed with sterile needle and syringe and 0.5 N HCl-extractable Fe(II), ferrozine-
176 extractable Fe(II), aqueous Fe(II), $NaHCO_3$-extractable U(VI), and aqueous U(VI)
177 concentrations were quantified as described below. All sample manipulations were
178 performed inside an anoxic chamber (95:5% N_2:H_2 atm; Coy Laboratory Products Inc.;
179 Grass Lake, MI).

180 **2.5. Experiments with biogenic uraninite and nontronite**

181 Biogenic uraninite ($UO_{2(s)}$) precipitates produced by MR-1 in experiments
182 conducted with 1.0 mM uranyl acetate as the sole electron acceptor (5 mM sodium lactate
183 in 30 mM $NaHCO_3$ buffer) were collected after a 50 d incubation period. The cell-
184 uraninite precipitates were pasteurized (70 ^oC for 30 min) to deactivate biological activity,
185 concentrated by centrifugation, and resuspended in anoxic 30 mM $NaHCO_3$. Nontronite
186 was dispensed into anoxic 30 mM $NaHCO_3$ in 20 mL glass serum bottles (5.0 g L^{-1},
187 99.4% Fe(III)). Abiotic uranium(IV) oxidation experiments were initiated by the
188 addition of 0.14 mM U(IV) as uraninite. Samples were periodically removed with sterile
189 needle and syringe (in anoxic chamber) and $NaHCO_3$-extractable U(VI) and aqueous
190 U(VI) concentrations were measured. A nontronite-free control was prepared along with
191 this experiment.

2.6. Experiments with chemically-reduced nontronite

Uranyl acetate was reacted with chemically-reduced nontronite to evaluate the rate and extent of U(VI) reduction by nontronite-Fe(II). Low-temperature oxygen traps were used to remove trace concentrations of dissolved oxygen from all reactant solutions and experimental reactors (Jeon et al., 2004a). Nontronite was reduced using the sodium citrate, bicarbonate, and dithionite (CBD) method as described by Stucki et al. (1984). Chemically-reduced nontronite was washed three times with anoxic distilled water as described by Hofstetter et al. (2003) and resuspended in anoxic 30 mM $NaHCO_3$ to yield a CBD-reduced nontronite stock suspension of 25 g L^{-1}. The CBD reduction period was purposefully controlled (Komadel et al., 1990) such that 27 % of the Fe(III) in nontronite was reduced to 0.5 N HCl-extractable Fe(II), a reduction extent comparable to the maximum extent in our bioreduction experiments. CBD-reduced nontronite was dispensed into anoxic 30 mM $NaHCO_3$ in 20 mL glass serum bottles (2.5 g L^{-1} final concentration, 2.8 mM 0.5 N HCl-extractable Fe(II)), and equilibrated at least 3 d before uranium addition. Abiotic uranium(VI) reduction experiments were initiated by the addition of 0.23 mM uranyl acetate to these bottles. Samples were periodically removed with sterile needle and syringe (in anoxic chamber) and 0.5 N HCl-extractable Fe(II), ferrozine-extractable Fe(II), aqueous Fe(II), $NaHCO_3$-extractable U(VI), and aqueous U(VI) concentrations were measured. All experiments were conducted in the dark at room temperature with no mixing except for sample collection. A uranium-free control was prepared along with this experiment.

2.7. Analytical techniques

Aqueous Fe(II) was measured after centrifugation for 10 min at 14,100 g and 20 ^{o}C, and analyzed using the ferrozine assay (Stookey, 1970; Royer et al., 2002). Ferrozine-extractable Fe(II) was measured after 0.1 mL of well-mixed suspension was added to 0.9 mL of anoxic ferrozine solution for 2 hours, centrifuged, and analyzed using the ferrozine assay. The ferrozine reagent (1.96 mM ferrozine in 50 mM HEPES, pH 8.0) does not dissolve nontronite (data not shown). We assume that ferrozine can extract Fe(II) adsorbed to clay surfaces, a fraction of the Fe(II) cation-exchanged in the clay interlayers, and the Fe(II) adsorbed to cell surfaces. We have operationally defined the difference between ferrozine-extractable and aqueous Fe(II) concentrations as "surface-adsorbed Fe(II)." 0.5 N HCl-extractable Fe(II) was measured after 0.5 mL of suspension was added to 0.5 mL of 1 N HCl for 24 h, centrifuged, and analyzed using the ferrozine assay. In previous studies it has been assumed that 0.5 N HCl can extract essentially all of the Fe(II) from the clay structure (Kostka et al., 1999a; Kostka et al., 1999b; O'Reilly et al., 2006; Furukawa and O'Reilly, 2007; Jaisi et al., 2007a; Zhang et al., 2007a; Zhang et al., 2007b), however, Jaisi et al. (2007b) have reported that 0.5 N HCl extracted only 73 % of total biogenic Fe(II) in NAu-2 compared to a HF/H_3PO_4 total dissolution method. Therefore, using select split samples, we compared the extraction efficiency of 0.5 N HCl to valence state determinations based on Fe X-ray absorption near edge structure (XANES) spectroscopy (described below). For bioreduced and re-oxidized samples (NUR and NUO), the Fe(II)/{Fe(II) + [Fe(III)]} ratios based on 0.5 N HCl extraction were equal to approximately 74 % of the Fe(II) ratios determined by linear combination fitting Fe XANES analysis (Table 2). Therefore, we assume that 0.5 N HCl can extract

236 only ca. 74 % of the Fe(II) from the clay structure, in good agreement with Jaisi et al
237 (2007b).

238 Aqueous U(VI) was measured after centrifugation for 10 min at 14,100 g and 20
239 ^{o}C. $NaHCO_3$-extractable U(VI) was measured in samples of well-mixed suspensions that
240 were placed in 1 M anoxic $NaHCO_3$ (pH 8.4) (all sample collection and manipulations
241 performed in anoxic chamber) (Elias et al., 2003; Zhou and Gu, 2005). After extraction
242 for 1 hr, solids were removed by centrifugation and U(VI) was measured in the
243 supernatant. U(VI) was measured by kinetic phosphorescence analysis on a KPA-11
244 (ChemChek Instruments, Richland, WA) (Brina and Miller, 1992). Adsorbed U(VI) was
245 operationally defined as the difference between $NaHCO_3$-extractable and aqueous U(VI)
246 concentrations, divided by the nontronite concentration. U valence state determinations
247 based on U XANES spectroscopy were in good agreement with the 1 M $NaHCO_3$
248 extraction data (Table 2).

249 **2.8. Electron microscopy**

250 Scanning electron microscopy (SEM) samples were prepared in an anoxic
251 glovebox following a previously published procedure (Zhang et al., 2007a). Briefly, cell-
252 mineral suspensions were fixed in anoxic 2.5% glutaraldehyde, placed on a glass cover
253 slip, and mineral particles were allowed to settle onto the cover slip for 15 min. The
254 particle-coated cover slips were gradually dehydrated in an ethanol series followed by
255 critical point drying (CPD). All sample preparation, except CPD, was performed in an
256 anoxic chamber. Cover slips were mounted onto a SEM stub and Au coated for
257 observation using a Zeiss Supra 35 FEG-VP SEM at an accelerating voltage of 10 to 15
258 kV. A short working distance (6 -10 mm) and low beam current (30 – 40 mA) were used

to achieve the best image resolution. A longer working distance (8.0 mm) and higher beam current (50 – 70 mA) were used for energy dispersive spectroscopy (EDS) analysis.

2.9. X-ray absorption spectroscopy

XAS measurements were made at the Materials Research Collaborative Access Team (MR-CAT) sector 10-ID beamline (Segre et al., 2000) of the Advanced Photon Source at Argonne National Laboratory (ANL). The XAS spectra were collected in transmission mode using quick-scanning of the monochromator. XANES spectra from the cell-uranium-nontronite precipitates were used to determine the average valence state of uranium and iron within the samples. For uranium and iron, the X-ray absorption edge energy was calibrated by collecting the reference spectrum from hydrogen uranyl phosphate (U(VI) Std) and an iron foil (Fe(0) Std), respectively, during the collection of each spectrum. All data sets were accurately aligned in energy using the derivative of the edge of the U(VI) or Fe(0) standard. A linear combination fitting (LCF) of the U(VI) Std and a biogenic nanoparticulate UO_2 standard (U(IV) Std) (O'Loughlin et al., 2003) was used to determine the approximate U(VI) to U(IV) ratio in the sample spectra. This approach assumes that the standard spectra represent the uranyl species in the samples. This assumption can lead to a systematic uncertainty for these samples because we do not know the U(VI) species. Similarly, the Fe XANES spectra were modeled with linear combinations of an Fe(II) standard spectrum from a fully reduced Fe(II)-nontronite NAu-2 and an Fe(III) standard spectrum from an unaltered fully oxidized Fe(III)-nontronite NAu-2. To further validate the valence state of the Fe in the Fe(III)-nontronite, the spectrum was modeled with a combination of Fe(III) oxide standards.

282 Samples (approximately 40 mg cell-uranium-nontronite precipitates) were
283 mounted as a moist paste on filter paper and covered with Kapton film and sealed with
284 Kapton tape. All sample preparation was performed in a Coy anoxic chamber and all
285 samples were stored in the chamber prior to analysis. Samples mounted in the holders
286 were exposed to the atmosphere for less than 1 min before being mounted for XAS
287 measurements in a free-flowing N_2 environment to limit possible sample oxidation.
288 These XAS sample holders have been shown to maintain anoxic integrity when exposed
289 to an oxic environment for at least 8 h (O'Loughlin et al., 2003). Uranium and iron
290 XANES spectra were collected in 30 second intervals consecutively for 5 minutes. No
291 radiation-induced changes to the XANES spectra were observed at the 30 second
292 intervals of data collection.

293 **3. RESULTS**

294 **3.1. U(VI) Speciation and Nontronite Dissolution**

295 The speciation of uranyl(VI) is sensitive to the concentrations of dissolved
296 calcium and magnesium (Fig. 1; Brooks et al., 2003; Dong and Brooks, 2006; Dong and
297 Brooks, 2008). While nontronite NAu-2 was prepared in a Na-saturated form, Ca and
298 Mg were detected in nontronite suspensions (5.0 g NAu-2 L^{-1}; anoxic 30 mM $NaHCO_3$
299 buffer, pH 6.8) before and after inoculation with *Shewanella putrefaciens* CN32 in
300 previous experiments very similar to those presented here (Table 3; Zhang et al., 2007a).
301 PHREEQC (Parkhurst et al., 1999) was used to model U(VI) speciation in 30 mM
302 $NaHCO_3$ with variable concentrations of Ca and Mg – 0 mM Ca and 0 mM Mg assumed
303 in the absence of nontronite; 0.06 mM Ca and 0.68 mM Mg measured with nontronite at
304 the start of the bioreduction period, and; 0.27 mM Ca and 1.16 mM Mg measured with

305 nontronite after a 23 d bioreduction period with CN32. Details of the U(VI) speciation
306 modeling are included in Electronic Annex EA-1. Ca and Mg were not measured as part
307 of our current experiments conducted with *Shewanella oneidensis* MR-1. With the lower
308 concentrations of Ca and Mg measured before bioreduction, $UO_2(CO_3)_3^{4-}$ was the
309 predominant U(VI) species accounting for 39 to 67 % of dissolved U(VI) species for total
310 U concentrations of 10 to 1,000 μM, respectively (Fig. 1b). With the higher
311 concentrations of Ca and Mg measured after bioreduction, $CaUO_2(CO_3)_3^{2-}$ became the
312 predominant U(VI) species below ca. 600 μM U(VI) (Fig. 1c).
313 0.5 N HCl-extractable Fe(II) concentrations were measured along with soluble Ca,
314 Mg, Si, Al and Fe_T during nontronite bioreduction by CN32 (Table 3; Zhang et al.,
315 2007a). Based on these evolving concentrations of soluble Fe, Mg, Si and Al during
316 bioreduction, congruent reductive dissolution of nontronite (Eq. 1 in Table 1) likely did
317 not occur. The final reduction extent reported in Table 3 is very similar to reduction
318 extents measured in our current experiments (Fig. 3 – 5). While a certain amount of Fe(II)
319 was released into solution, the majority of Fe(II) was retained in the clay structure. As
320 noted in section 2.7, we assume that 0.5 N HCl can extract ca. 74 % of the Fe(II) from the
321 nontronite structure as supported by Fe XANES spectroscopy measurements for select
322 samples (Table 2).
323 **3.2. U(VI) Sorption onto Nontronite**
324 The sorption of uranyl onto nontronite was dependent on both the pH and ionic
325 strength of the background electrolyte (Fig. 2a). The pH effect was caused by both
326 changes in uranyl speciation and nontronite surface charge as a function of pH. While
327 U(VI) speciation is sensitive to Ca and Mg, because these metals were not measured as a

328 function of pH during the sorption experiments, Ca-U(VI)-CO_3 and Mg-U(VI)-CO_3
329 species were not included in reaction networks used for speciation modeling of the
330 sorption edges (Electronic Annex EA-1). For a solution of 10 μM U(VI) in 0.01 M
331 $NaNO_3$ (in equilibrium with atmospheric CO_2), U(VI) speciation modeling demonstrated
332 that cationic uranyl species were predominant up to ca. pH 5.5, and that anionic uranyl
333 species were predominant at pH values above ca. pH 6.0. Nontronite contains both a
334 permanent negative layer charge and a pH-dependent edge charge. Structural Fe(III) in
335 the octahedral layer (92 % Fe_T) imparts no layer charge (Fe^{3+} substituted for Al^{3+}),
336 however, structural Mg(II) substituted for Al^{3+} imparts a permanent negative charge.
337 Structural Fe(III) in the tetrahedral layer (8 % Fe_T) imparts a permanent negative charge
338 (Fe^{3+} substituted for Si^{4+}) to basal siloxane surfaces.
339 The pH-dependent edge charge is located at the layer edges and is regulated by
340 surface hydroxyl groups. The pH at zero point of charge (pH_{zpc}) for nontronite has been
341 reported to range from pH 6.5 (Merola et al., 2007) to pH 7.0 (Jaisi et al., 2007a),
342 therefore, nontronite was likely predominantly positively charged below ca. pH 5.5 and
343 predominantly negatively charged above ca. pH 8.0. Complexation to edge sites is not
344 favorable at low pH because H^+ can out-compete UO_2^{2+} for sorption sites. Furthermore,
345 the predominant sorption mechanism onto nontronite at low pH is presumed to be cation
346 exchange to basal siloxane surfaces (Boult et al., 1998; Kowal-Fouchard et al., 2004),
347 consistent with our results that showed higher Na^+ concentrations suppressed UO_2^{2+} at
348 low pH. The sorption of uranyl to nontronite was relatively constant between pH 6.0 –
349 8.0 and independent of ionic strength, suggesting that neutral (UO_2CO_3) and polymeric
350 ($(UO_2)_2CO_3(OH)_3^-$) species could sorb strongly (e.g., as inner sphere complexes) under

351 these conditions. Catalano and Brown (2005) used EXAFS spectroscopy to show that
352 $UO_2(CO_3)^{4-}_{3(aq)}$ was preferentially bound to $[Fe(O,OH)_6]$ octahedral sites over
353 $[Al(O,OH)_6]$ octahedral sites on layer edge sites of smectite. Because nontronite has very
354 low aluminum content in octahedral sites (Keeling et al., 2000), we speculate that
355 $[Fe(O,OH)_6]$ octahedral layer edge sites play a predominant role in uranyl sorption to
356 nontronite.

357 The extent of uranyl sorption onto nontronite at pH 6.8 in anoxic 30 mM $NaHCO_3$
358 was measured to quantify the distribution of U(VI) under the conditions used in the
359 bioreduction experiments (Fig. 2b). We assumed that 0.06 mM Ca and 0.68 mM Mg
360 dissolved from nontronite under this one pH condition (Table 3). Depending on the
361 initial U(VI) concentration (0.025 – 1.5 mM), 13.3 – 24.6 % of the total U(VI) was
362 sorbed onto nontronite (5.0 g L^{-1}). The predominant uranyl species for all the sorption
363 experiments in 30 mM $NaHCO_3$ was $UO_2(CO_3)_3^{4-}$ (Fig. 1b). Uranyl surface coverage
364 achieved a maximum value of $1.73*10^{-3}$ mole m^{-2} (equivalent to1.04 sites nm^{-2}) at the
365 highest U(VI) concentration tested. The maximum sorption density of Fe(II) onto
366 nontronite (5.0 g L^{-1}) at pH 6.8 in anoxic 30 mM PIPES buffer was reported to equal 17
367 sites nm^{-2} (Jaisi et al., 2007c). The differences in sorption density of Fe(II) versus U(VI)
368 was likely due to the strong complexation of UO_2^{2+} by carbonate under these conditions.
369 Based on our review of the literature, the sorption of uranyl onto nontronite has been
370 reported only one other time (Ames et al., 1983) (Table 4). From results reported by
371 Ames et al. (1982), we calculated a uranyl sorption density of $3.34*10^{-3}$ mole m^{-2} for
372 their experiments conducted at pH 7.7 in Hanford groundwater with a natural smectite
373 (experiments in equilibrium with atmospheric CO_2). For uranyl sorption onto

montmorillonite SWy-2, a sorption density of $9.57*10^{-3}$ mole m^{-2} was reported for experiments conducted at pH 7.1 in 100 mM $NaNO_3$ (Pabalan and Turner, 1997; Prikryl et al., 2001).

3.3. Bioreduction of U(VI) and Nontronite

Shewanella oneidensis MR-1 was able to reduce both uranyl(VI) and structural Fe(III) in nontronite when both of these TEAs were present (Fig. 3; $0.5*10^8$ cell mL^{-1}). In the absence of nontronite or AQDS, U(VI) was removed relatively slowly from solution but was effectively removed to <5 μM after 21 days. The addition of the soluble electron shuttle AQDS increased the rate of U(VI) removal. In the presence of nontronite (but absence of AQDS), U(VI) was not effectively removed at a cell density of $0.5*10^8$ cell mL^{-1} even though substantial Fe(II) had evolved (Fig. 3b). However, when AQDS was later added to U(VI)-with-nontronite suspensions, complete removal of U(VI) occurred rapidly. In the presence of U(VI), nontronite and AQDS, bioreduction of nontronite occurred most rapidly and to the greatest extent, and U(VI) removal kinetics were faster compared to suspensions of U(VI)-with-nontronite and U(VI) alone. The addition of AQDS was previously shown to significantly increase the rate and extent of nontronite bioreduction (Dong et al., 2003).

With a near-constant initial concentration of U(VI) (0.7 – 0.8 mM), increasing concentrations of nontronite increased the lag time prior to U(VI) reduction but did not inhibit the ultimate removal of U(VI) (Fig. 4; $1.0*10^8$ cell mL^{-1}). The extent of nontronite reduction in our experiments was measured only after 27 and 52 days. After a 52 day incubation with variable nontronite concentrations, the extent of U(VI) removal was near-constant and complete, while the extent of nontronite reduction (expressed as %

397 of Fe_T) decreased with increased clay concentrations (Fig. 4b). With a constant initial
398 concentration of nontronite (5.0 g L^{-1}), increasing concentrations of U(VI) increased the
399 rate and extent of nontronite reduction, however, this enhancement effect began to
400 decline at U(VI) concentrations above 800 μM (Fig. 5; $1.0*10^8$ cell mL^{-1}). The extent of
401 U(VI) reduction in these experiments was measured only after 27 and 52 days. After a
402 52 day incubation with variable U(VI) concentrations, the extent of nontronite reduction
403 was near-constant (ca. 30 %) except for 0 and 1500 μM U(VI) concentrations, while the
404 extent of U(VI) removal was relatively low at the lowest (25 – 100 μM) and highest
405 (1500 μM) U(VI) concentrations but essentially complete at intermediate U(VI)
406 concentrations (400 – 1000 μM) (Fig. 5b).

407 **3.4. Abiotic Oxidation of Biogenic Uraninite by Nontronite**

408 Biogenic uraninite was effectively oxidized by structural Fe(III) in nontronite
409 when reacted in anoxic 30 mM $NaHCO_3$ (Fig. 6). Complete re-oxidation of uraninite to
410 U(VI) occurred in ca. 1.2 days. Structural Fe(III) in nontronite oxidized biogenic
411 uraninite at rates comparable to uraninite oxidation by poorly crystalline Fe(III)
412 (oxyhydr)oxides (Senko et al., 2005; Ginder-Vogel et al., 2006). The rate of uraninite
413 oxidation was quantified as the rate of soluble U(VI) production according to:

414 $$R_{ox} = d[UO_2]/dt = -k_{ox}\cdot([U_{TOT}] - [U(VI)(sol)]) \quad (1)$$

415 where k_{ox} is the pseudo-first-order oxidation rate constant (d^{-1}) and $[U_{TOT}]$ is the total
416 uranium concentration (both U(IV) and U(VI)) in the reactor. The rate constant for
417 nontronite-Fe(III) oxidation of uraninite was 1.14 d^{-1} ($R^2 = 0.96$), and was measured
418 using identical procedures developed in our previous experiments on the oxidation of
419 biogenic uraninite (Burgos et al., 2008). In those experiments, uraninite was produced by

S. oneidensis MR-1 in 30 mM $NaHCO_3$ and subsequently oxidized by dissolved oxygen. The values for k_{ox} for uraninite oxidation by dissolved oxygen were found to vary from 16 to 27 d^{-1}. While these two sets of experiments were not conducted side-by-side with identical materials, it appears that dissolved oxygen will react more rapidly than nontronite-Fe(III) in the oxidation of uraninite. This is not unexpected considering that oxygen is a stronger oxidant than structural Fe(III) and, as a dissolved constituent, would have greater access to uraninite particles.

3.5. Abiotic Reduction of U(VI) by Chemically-Reduced Nontronite

Uranyl was only partially removed from solution in the presence of citrate-dithionite-bicarbonate (CBD)-reduced nontronite (Fig. 7), even in the presence of a large stoichiometric excess of Fe(II) relative to U(VI). In preparing the CBD-reduced nontronite, the extent of reduction, 27 % Fe(II) (equivalent to 2.8 mM 0.5 N HCl-extractable Fe(II)), was purposefully controlled (Komadel et al., 1990) to be comparable to maximum reduction extents achieved in the bioreduction experiments. The CBD-reduced nontronite was washed three times with anoxic distilled water such that Ca concentrations were likely low (e.g., << 0.06 mM). Surface-adsorbed Fe(II) concentrations remained relatively constant, ranging from 75 to 100 μM (equivalent to 2.7 – 3.6 % of 0.5 N HCl-extractable Fe(II) in system), and aqueous Fe(II) concentrations ranged from 10 to 30 μM. Structural Fe(II) was the predominant reductant in this system. The $NaHCO_3$-extractable U(VI) concentration decreased from 230 to 180 μM between days 1 and 4 in conjunction with a decrease in the of 0.5 N HCl-extractable Fe(II) concentration. However, the decrease and subsequent increase in the 0.5 N HCl-extractable Fe(II) concentration could not be solely attributed to changes in U(VI)

443 concentrations, suggesting that other redox active components could have been present in
444 these suspensions. The use of low-temperature O_2-traps in the preparation and
445 maintenance of all reactant solutions used in these experiments would lead us to believe
446 that O_2 was not significant in these incubations. Regardless of the time-dependent
447 behavior of 0.5 N HCl-extractable Fe(II), both structural and surface-adsorbed Fe(II)
448 species were present and yet the total U(VI) concentration was not statistically different
449 from 4 to 82 days ($t = -19.8$; $p = 0.0001$).

450 **3.6. Characterization of Mineral Products**

451 Mineral products from many of these experiments were characterized by XRD,
452 SEM, and XANES spectroscopy. The presence of nontronite did not substantially affect
453 the XRD patterns of biogenic uraninite (Electronic Annex EA-2), even though uraninite
454 and nontronite were observed in close proximity in SEM images (Fig. 8b,c). In the
455 absence of nontronite, a predominant portion of uraninite accumulated extracellularly of
456 MR-1 (Fig. 8a). In the presence of nontronite, MR-1 cells were found to associate with
457 both nontronite and uraninite. MR-1 cells were not found preferentially associated with
458 any specific facet of the nontronite particles (e.g., along layer edges or basal siloxane
459 surfaces). Nontronite particles collected at the end of the bioreduction experiment
460 exhibited severe dissolution features (Fig. 8d). SEM-EDS analyses revealed increased
461 uranium content with bioreduced nontronite particles, presumably nanoparticulate
462 uraninite, that was not observed in abiotic U(VI)-with-nontronite controls. Broad
463 diffraction peaks for biogenic uraninite were indicative of fine-grained nanoparticulate
464 uraninite, consistent with our SEM observations.

465 The biological reduction of nontronite affected the XRD patterns of these clays
466 compared to the initial unaltered material (Electronic Annex EA-2). Bioreduction of
467 Fe(III) in nontronite resulted in the disappearance of the peak at 12.8 Å (2θ = 6.9°) and
468 appearance of peaks at 15.2 Å (2θ = 5.8°) and 12.4 Å (2θ = 7.1°). The dissolution of
469 nontronite caused by bioreduction was consistent with previous studies that, either
470 directly or indirectly, observed collapsed nontronite layers upon reduction (Lear and
471 Stucki, 1989; Wu et al., 1989; Kostka et al., 1999a; Dong et al., 2003; Zhang et al.,
472 2007b).
473 The average oxidation state of both Fe and U were determined by XANES
474 spectroscopy for select samples collected during these experiments. XANES spectra
475 were collected from abiotic controls (1.0 mM U(VI), 5.0 g L^{-1} nontronite) that had been
476 incubated for 52 days, biotic controls inoculated with $1.0*10^{8}$ cell mL^{-1} MR-1 and
477 incubated for 52 days (Fig. 4), and the biotic controls after they were oxidized by
478 dissolved oxygen for 20 h. The Fe K edge XANES spectrum for the bioreduced sample
479 was intermediate between our Fe(III) and Fe(II) nontronite NAu-2 standards (sample
480 NUR in Fig. 9a). The Fe(II)/Fe(III) ratio was determined by linear combination fitting
481 (LCF) as described in section 2.9. The Fe reduction extent calculated as ([Fe(II)]/{[Fe(II)]
482 + [Fe(III)]}) was 38 ± 10 % compared to our estimate of 28.3 % based on Fe(II)
483 measured after 0.5 N HCl extraction (Table 2). The Fe(II)/Fe_T ratio of the abiotic control
484 was 0 ± 10 %, in good agreement with the 0.5 N HCl extraction measurement (0.38 ±
485 3.0 %). The U L_{III} edge XANES spectra for the bioreduced sample closely matched that
486 of a U(IV) standard of biogenic UO_2 nanoparticles (Fig. 9b). The U(IV)/U(VI) ratio was
487 determined by LCF of the XANES spectra. The U reduction extent calculated as

488 ([U(IV)]/{[U(IV)] + [U(VI)]}) was 90 ± 10 % in good agreement with our estimate of 83
489 ± 2.7 % based on total U(VI) measured after 1 M $NaHCO_3$ extraction (Table 2).

490 **4. DISCUSSION**

491 The biologic and abiotic reactions between DMRB, nontronite and uranium
492 represent a series of complex, coupled processes (Fig. 10). In the current experiments we
493 found that U(VI) enhanced the rate and extent of nontronite-Fe(III) reduction (Fig. 3 – 5),
494 and that uraninite oxidation by structural Fe(III) in nontronite was relatively fast (Fig. 6).
495 The relatively rapid reoxidation of U(IV) allows uranium to serve as an effective electron
496 shuttle to nontronite-Fe(III). We also found that U valence cycling was driven primarily
497 by biological reduction because abiotic reduction of U(VI) by CBD-reduced nontronite-
498 Fe(II) was thermodynamically unfavorable or kinetically limited (Fig. 7). An important
499 finding from this work with respect to engineered systems for *in situ* immobilization of
500 uranium is that iron-rich clays may inhibit the goal of U removal from solution. Indeed
501 we observed that increasing concentrations of nontronite increased the lag time prior to
502 U(VI) reduction (Fig. 4).

503 A mechanistic description of the operative reactions in these experimental
504 systems requires an understanding of U(VI) speciation and the reactive forms of Fe(II).
505 The redox behaviors of the U(VI)/U(IV) couple and the nontronite-Fe(III)/Fe(II) couple
506 are relatively complex and strongly dependent on chemical activities and bulk
507 geochemical conditions. While the thermodynamics of uranium geochemistry are well
508 established, the thermodynamic properties of iron-rich smectites like nontronite are less
509 constrained. For example, reduction potentials for nontronite are often written as
510 congruent dissolution reactions (Eq. 1 in Table 1) while it is known that the majority of

511 reduced Fe(II) remains in the clay structure. Thus, Fe(II) can exist in a variety of forms
512 in reduced nontronite suspensions, each of which may have a distinct but unknown
513 reduction potential. We envision that Fe(II) in these systems can exist in the octahedral
514 and tetrahedral layers of the clay, complexed to layer edge sites, sorbed to basal siloxane
515 surfaces, or dissolved in solution.

516 Nontronite dissolution or cation exchange reactions can also lead to the
517 introduction or alteration of dissolved concentrations of Ca and Mg. These two cations
518 have particularly important effects on uranium speciation and reactivity (Brooks et al.
519 2003; Dong and Brooks, 2006; Dong and Brooks, 2008). As shown in Fig. 1, U(VI)
520 speciation is significantly altered with the addition of just 0.06 mM Ca. The shift of the
521 predominant U(VI) species from $UO_2(CO_3)_3^{4-}$ to $CaUO_2(CO_3)_3^{2-}$ could affect sorption
522 and redox reactions with nontronite. Using published values of standard-state reduction
523 potentials (E^0) for these U(VI) species (Table 1), effective reduction potentials (E'_{red})
524 were calculated for the current experimental conditions. The following conditions were
525 selected for comparison purposes: 25 ^oC, pH 6.8, 30 mM $NaHCO_3$, 500 μM $UO_2(CO_3)_3^{4-}$
526 with no Ca present or 500 μM $CaUO_2(CO_3)_3^{2-}$ with 0.27 mM Ca. For these conditions,
527 $UO_2(CO_3)_3^{4-}$ has an E'_{red} of +0.12 V, while $CaUO_2(CO_3)_3^{2-}$ has an E'_{red} of +0.22 V. Thus,
528 while Ca does affect U(VI) speciation, it does not decrease the reduction potential of
529 other predominant U(VI) species. If the Ca concentration increased to 10 mM,
530 $CaUO_2(CO_3)_3^{2-}$ has an E'_{red} of +0.13 V.

531 Selection of a redox couple for nontronite-Fe(III)/Fe(II) is more challenging
532 compared to U(VI)/U(IV). On one hand, a redox couple that represents reduction
533 without dissolution for structural nontronite-Fe(III)/structural nontronite-Fe(II) (Eq. 2 in

534 Table 1; Favre et al., 2006) is appealing because the majority of Fe(II) does indeed
535 remain in the clay structure. However, calculation of the reduction potential as a function
536 of reaction extent is problematic due to the assignment of chemical activities to these
537 solid-phase species. On the other hand, a redox couple that represents congruent
538 dissolution for structural nontronite-Fe(III)/Fe^{2+}(aq) (Eq. 1 in Table 1; Jaisi et al. 2007b)
539 is appealing because the reduction potential of the remaining nontronite-Fe(III) can be
540 calculated directly from aqueous metal concentrations. However, as noted above,
541 congruent dissolution of nontronite does not commonly occur.
542 The bioreduction of $UO_2(CO_3)_3^{4-}$ coupled to lactate oxidation has an effective
543 overall reduction potential ($E'_{overall}$) of +0.59 V with an initial U(VI) concentration of
544 1,000 uM, 5 mM lactate, and 2 mM acetate (from $UO_2(Ace)_2$). In comparison, the
545 bioreduction of nontronite-Fe(III) (using Eq. 1 in Table 1) coupled to lactate oxidation
546 has an $E'_{overall}$ of +0.97 V with an initial Fe(II) concentration of 1 uM and a lactate/acetate
547 ratio of 5/2. Therefore, the bioreduction of nontronite-Fe(III) was thermodynamically
548 favorable compared to U(VI) bioreduction in these experimental systems. However, in
549 experiments conducted with sole electron acceptors, both the rate and extent of electron
550 acceptor utilization was greater with U(VI) compared to nontronite-Fe(III). Due to
551 kinetic constraints related to transferring electrons to a solid-phase electron acceptor,
552 U(VI) was likely reduced before nontronite-Fe(III).
553 With these conceptual thermodynamic calculations and experimental observations,
554 we propose that U valence cycling in these systems can be explained as follows (Fig. 10):
555 DMRB preferentially bioreduce soluble U(VI) over solid-phase nontronite-Fe(III);
556 uraninite is rapidly reoxidized by nontronite-Fe(III) at the start of the experiments; as

557 Fe^{2+}(aq) or structural Fe(II) accumulate in the system, the reduction potential of
558 nontronite-Fe(III) decreases; at some elevated concentration of Fe(II), nontronite-Fe(III)
559 can no longer oxidize uraninite; DMRB continue to bioreduce U(VI), however, now it
560 remains as uraninite and finally precipitates from solution. The lag phase for the onset of
561 U(VI) loss from solution increased with increasing nontronite concentrations (Fig. 4).
562 Higher nontronite concentrations provide greater sorption capacity for Fe^{2+}, which delays
563 the increase in Fe^{2+}(aq) and, therefore, prolongs the lag phase. The important implication
564 of this is that U valence cycling with iron-rich clays may inhibit U removal from solution
565 in subsurface environments.
566
567 **Acknowledgements**
568 This work was supported by the Natural and Accelerated Bioremediation Research
569 (NABIR) Program, Office of Biological and Environmental Research (BER), Office of
570 Energy Research, U.S. Department of Energy (DOE) grant no. DE-FG02-01ER631180 to
571 The Pennsylvania State University, and by the National Science Foundation under Grant
572 No. CHE-0431328. Use of the MRCAT sector at the Advanced Photon Source (APS)
573 was supported by the Environmental Remediation Science Program (ERSP), U.S. DOE,
574 Office of Science, BER and the MRCAT member institutions. Use of the APS was
575 supported by the U.S. Department of Energy, Office of Science, Office of Basic Energy
576 Sciences, under contract DE-AC02-06CH11357. We thank Ed O'Loughlin for preparing
577 and providing nontronite-Fe(III) and nontronite-Fe(II) standards for XANES
578 spectroscopy. We thank Jeff Catalano and two anonymous reviewers for providing
579 helpful comments that improved this manuscript.
580

581 **References**

582 Ames L. L., Mcgarrah J. E., and Walker B. A. (1982) Sorption of Uranium and Cesium
583 by Hanford Basalts and Associated Secondary Smectite. *Chemical Geology* 35,
584 205-225.
585 Ames L. L., Mcgarrah J. E., and Walker B. A. (1983) Sorption of trace constituents from
586 aqueous solutions onto secondary minerals. I. Uranium. *Clays and Clay Minerals*
587 31(5), 321-334.
588 Anderson R. T., Vrionis H. A., Ortiz-Bernad I., Resch C. T., Long P. E., Dayvault R.,
589 Karp K., Marutzky S., Metzler D. R., Peacock A., White D. C., Lowe M., and
590 Lovley D. R. (2003) Stimulating the in situ activity of Geobacter species to
591 remove uranium from the groundwater of a uranium-contaminated aquifer.
592 *Applied and Environmental Microbiology* 69(10), 5884-5891.
593 Behrends T. and Van Cappellen P. (2005) Competition between enzymatic and abiotic
594 reduction of uranium(VI) under iron reducing conditions. *Chemical Geology*
595 220(3-4), 315-327.
596 Boult K. A., Cowper M. M., Heath T. G., Sato H., Shibutani T., and Yui M. (1998)
597 Towards an understanding of the sorption of U(V) and Se(IV) on sodium
598 bentonite. *Journal of Contaminant Hydrology* 35(1-3), 141-150.
599 Brina R. and Miller A. G. (1992) Direct Detection of Trace Levels of Uranium by Laser-
600 Induced Kinetic Phosphorimetry. *Analytical Chemistry* 64(13), 1413-1418.
601 Brooks S. C., Fredrickson J. K., Carroll S. L., Kennedy D. W., Zachara J. M., Plymale A.
602 E., Kelly S. D., Kemner K. M., and Fendorf S. (2003) Inhihition of bacterial U(VI)
603 reduction by calcium. *Environmental Science & Technology* 37(9), 1850-1858.
604 Catalano J. G., and Brown G. E. (2005) Uranyl adsorption onto montmorillonite:
605 Evaluation of binding sites and carbonate complexation. *Geochimica Et*
606 *Cosmochimica Acta* 69(12), 2995-3005.
607 Dong H., Kostka J. E., and Kim J. W. (2003) Microscopic evidence for microbial
608 dissolution of smectite. *Clays and Clay Minerals* 51(5), 502-512.
609 Dong W., and Brooks S. C. (2006) Determination of the Formation Constants of Ternary
610 Complexes of Uranyl and Carbonate with Alkaline Earth Metals (Mg^{2+}, Ca^{2+}, Sr^{2+},
611 and Ba^{2+}) Using Anion Exchange Method. *Environ. Sci. Technol.* **40**(15), 4689-
612 4695.
613 Dong W., and Brooks S. C. (2008) Formation of Aqueous $MgUO_2(CO_3)_3^{2-}$ Complex and
614 Uranium Anion Exchange Mechanism onto an Exchange Resin. *Environ. Sci.*
615 *Technol.* **42**(6), 1979-1983.
616 Elias D. A., Senko J. M., and Krumholz L. R. (2003) A procedure for quantitation of total
617 oxidized uranium for bioremediation studies. *Journal of Microbiological Methods*
618 53(3), 343-353.
619 Elsner M., Schwarzenbach R. P., and Haderlein S. B. (2004) Reactivity of Fe(II)-bearing
620 minerals toward reductive transformation of organic contaminants. *Environmental*
621 *Science & Technology* 38(3), 799-807.
622 Favre F., Stucki J. W., and Boivin P. (2006) Redox properties of structural Fe in
623 ferruginous smectite. A discussion of the standard potential and its environmental
624 implications. *Clays and Clay Minerals* 54(4), 466-472.

Fredrickson J. K., Zachara J. M., Kennedy D. W., Duff M. C., Gorby Y. A., Li S. M. W., and Krupka K. M. (2000) Reduction of U(VI) in goethite (alpha-FeOOH) suspensions by a dissimilatory metal-reducing bacterium. *Geochimica et Cosmochimica Acta* 64(18), 3085-3098.

Fredrickson J. K., Zachara J. M., Kennedy D. W., Liu C., Duff M. C., Hunter D. B., and Dohnalkova A. (2002) Influence of Mn oxides on the reduction of Uranium(VI) by the metal-reducing bacterium Shewanella putrefaciens. *Geochimica et Cosmochimica Acta* 66(18), 3247-3262.

Furukawa Y., and O'Reilly S. E. (2007) Rapid precipitation of amorphous silica in experimental systems with nontronite (NAu-1) and Shewanella oneidensis MR-1. *Geochimica et Cosmochimica Acta* 71(2), 363-377.

Gates W. P., Slade P. G., Manceau A., and Lanson B. (2002) Site occupancies by iron in nontronites. *Clays and Clay Minerals* 50(2), 223-239.

Ginder-Vogel M., Criddle C. S., and Fendorf S. (2006) Thermodynamic constraints on the oxidation of biogenic UO2 by Fe(III) (hydr) oxides. *Environmental Science & Technology* 40(11), 3544-3550.

Grenthe I., Stumm W., Laaksuharju M., Nilsson A. C., and Wikberg P. (1992) Redox potentials and redox reactions in deep groundwater systems. *Chemical Geology* 98(1-2), 131-150.

Hofstetter T. B., Neumann A., and Schwarzenbach R. P. (2006) Reduction of nitroaromatic compounds by Fe(II) species associated with iron-rich smectites. *Environmental Science & Technology* 40(1), 235-242.

Hofstetter T. B., Schwarzenbach R. P., and Haderlein S. B. (2003) Reactivity of Fe(II) species associated with clay minerals. *Environmental Science & Technology* 37(3), 519-528.

Istok J. D., Senko J. M., Krumholz L. R., Watson D., Bogle M. A., Peacock A., Chang Y. J., and White D. C. (2004) In situ bioreduction of technetium and uranium in a nitrate-contaminated aquifer. *Environmental Science & Technology* 38(2), 468-475.

Jaisi D. P., Dong H. L., and Liu C. X. (2007a) Kinetic analysis of microbial reduction of Fe(III) in nontronite. *Environmental Science & Technology* 41(7), 2437-2444.

Jaisi D. P., Dong H. L., and Liu C. X. (2007b) Influence of biogenic Fe(II) on the extent of microbial reduction of Fe(III) in clay minerals nontronite, illite, and chlorite. *Geochimica Et Cosmochimica Acta* 71(5), 1145-1158.

Jaisi D. P., Kukkadapu R. K., Eberl D. D., and Dong H. L. (2005) Control of Fe(III) site occupancy on the rate and extent of microbial reduction of Fe(III) in nontronite. *Geochimica Et Cosmochimica Acta* 69(23), 5429-5440.

Jeon B. H., Dempsey B. A., Burgos W. D., Barnett M. O., and Roden E. E. (2005) Chemical reduction of U(VI) by Fe(II) at the solid-water interface using natural and synthetic Fe(III) oxides. *Environmental Science & Technology* 39(15), 5642-5649.

Jeon B. H., Dempsey B. A., Royer R. A., and Burgos W. D. (2004a) Low-temperature oxygen trap for maintaining strict anoxic conditions. *Journal of Environmental Engineering-Asce* 130(11), 1407-1410.

669 Jeon B. H., Kelly S. D., Kemner K. M., Barnett M. O., Burgos W. D., Dempsey B. A.,
670 and Roden E. E. (2004b) Microbial reduction of U(VI) at the solid-water interface.
671 *Environmental Science & Technology* 38(21), 5649-5655.
672 Keeling J. L., Raven M. D., and Gates W. P. (2000) Geology and characterization of two
673 hydrothermal nontronites from weathered metamorphic rocks at the Uley
674 Graphite Mine, South Australia. *Clays and Clay Minerals* 48(5), 537-548.
675 Keller M. D., Bellows W. K., and Guillard R. R. L. (1988) Microwave Treatment for
676 Sterilization of Phytoplankton Culture Media. *Journal of Experimental Marine*
677 *Biology and Ecology* 117(3), 279-283.
678 Kostka J. E., Dalton D. D., Skelton H., Dollhopf S., and Stucki J. W. (2002) Growth of
679 iron(III)-reducing bacteria on clay minerals as the sole electron acceptor and
680 comparison of growth yields on a variety of oxidized iron forms. *Applied and*
681 *Environmental Microbiology* 68(12), 6256-6262.
682 Kostka J. E., Haefele E., Viehweger R., and Stucki J. W. (1999a) Respiration and
683 dissolution of iron(III)-containing clay minerals by bacteria. *Environmental*
684 *Science and Technology* 33, 3127-3133.
685 Kostka J. E., Wu J., Nealson K. H., and Stucki J. W. (1999b) The impact of structural
686 Fe(III) reduction by bacteria on the surface chemistry of smectite clay minerals.
687 *Geochimica et Cosmochimica Acta* 63(22), 3705-3713.
688 Kowal-Fouchard A., Drot R., Simoni E., and Ehrhardt J. J. (2004) Use of spectroscopic
689 techniques for uranium (VI)/montmorillonite interaction modeling.
690 *Environmental Science & Technology* 38(5), 1399-1407.
691 Lear P. R., and Stucki J. W. (1989) Effects of iron oxidation state on the specific surface
692 area of nontronite. *Clays & Clay Minerals* 37, 547-552.
693 Liger E., Charlet L., and Van Cappellen P. (1999) Surface catalysis of uranium(VI)
694 reduction by iron(II). *Geochimica Et Cosmochimica Acta* 63(19-20), 2939-2955.
695 Lovley, D. R. (1993) Dissimilatory Metal Reduction. *Annual Review of Microbiology* 47,
696 263-290.
697 Merola R. B., Fournier E. D., and Mcguire M. M. (2007) Spectroscopic investigations of
698 Fe2+ complexation on nontronite clay. *Langmuir* 23(3), 1223-1226.
699 Missana T., Garcia-Gutierrez M., and Fernndez V. (2003) Uranium(VI) sorption on
700 colloidal magnetite under anoxic environment: Experimental study and surface
701 complexation modelling. *Geochimica Et Cosmochimica Acta* 67(14), 2543-2550.
702 Nealson K. H. and Saffarini D. (1994) Iron and manganese in anaerobic respiration:
703 environmental significance, physiology, and regulation. *Annual Review of*
704 *Microbiology* 48, 311-343.
705 O'Loughlin E. J., Kelly S. D., Cook R. E., Csencsits R., and Kemner K. M. (2003)
706 Reduction of Uranium(VI) by mixed iron(II/iron(III) hydroxide (green rust):
707 Formation of UO2 manoparticies. *Environmental Science & Technology* 37(4),
708 721-727.
709 O'Reilly S. E., Furukawa Y., and Newell S. (2006) Dissolution and microbial Fe(III)
710 reduction of nontronite (NAu-1). *Chemical Geology* 235(1-2), 1-11.
711 Pabalan R. T., and Turner D. R. (1997) Uranium(6+) Sorption on Montmorillonite:
712 Experimental and Surface Complexation Modeling Study. *Aquatic Geochemistry*
713 2, 203-226.

714 Peretyazhko T., Zachara J. M., Heald S. M., Jeon B. H., Kukkadapu R. K., Liu C., Moore
715 D., and Resch C. T. (2008) Heterogeneous Reduction of Tc(VII) by Fe(II) at the
716 Solid-Water Interface. *Geochimica et Cosmochimica Acta* 72, 1521–1539.
717 Prikryl J. D., Jain A., Turner D. R., and Pabalan R. T. (2001) Uranium(VI) sorption
718 behavior on silicate mineral mixtures. *Journal of Contaminant Hydrology* 47(2-4),
719 241-253.
720 Royer R. A., Burgos W. D., Fisher A. S., Jeon B. H., Unz R. F., and Dempsey B. A.
721 (2002) Enhancement of hematite bioreduction by natural organic matter.
722 *Environmental Science & Technology* 36(13), 2897-2904.
723 Schwertmann U., and Cornell R. M. (2000) *Iron oxides in the laboratory; preparation*
724 *and characterization*. VCH-Wiley, Weinheim, Federal Republic of Germany
725 (DEU).
726 Senko J. M., Dewers T. A., and Krumholz L. R. (2005) Effect of oxidation rate and Fe(II)
727 state on microbial nitrate-dependent Fe(III) mineral formation. *Applied and*
728 *Environmental Microbiology* 71(11), 7172-7177.
729 Sorensen K. C., Stucki J. W., Warner R. E., Wagner E. D., and Plewa M. J. (2005)
730 Modulation of the genotoxicity of pesticides reacted with redox-modified smectite
731 clay. *Environmental and Molecular Mutagenesis* 46(3), 174-181.
732 Stookey L. L. (1970) Ferrozine-a new spectrophotometric reagent for iron. *Analytical*
733 *Chemistry* 42, 779-781.
734 Stucki J. W., Golden D. C., and Roth C. B. (1984) Effects of Reduction and Reoxidation
735 of Structural Iron on the Surface-Charge and Dissolution of Dioctahedral
736 Smectites. *Clays and Clay Minerals* 32(5), 350-356.
737 Wielinga B., Bostick B., Hansel C. M., Rosenzweig R. F., and Fendorf S. (2000)
738 Inhibition of bacterially promoted uranium reduction: Ferric (hydr)oxides as
739 competitive electron acceptors. *Environmental Science & Technology* 34(11),
740 2190-2195.
741 Wu J., Low P. F., and Roth C. B. (1989) Effects of octahedral-iron reduction and
742 swelling pressure on interlayer distances in Na-nontronite. *Clays and Clay*
743 *Minerals* 37(3), 211-218.
744 Wu W. M., Carley J., Fienen M., Mehlhorn T., Lowe K., Nyman J., Luo J., Gentile M. E.,
745 Rajan R., Wagner D., Hickey R. F., Gu B., Watson D., Cirpka O. A., Kitanidis P.
746 K., Jardine P. M., and Criddle C. S. (2006a) Pilot-Scale in Situ Bioremediation of
747 Uranium in a Highly Contaminated Aquifer. 1. Conditioning of a Treatment Zone.
748 *Environ. Sci. Technol.* 40(12), 3978-3985.
749 Wu W. M., Carley J., Gentry T., Ginder-Vogel M. A., Fienen M., Mehlhorn T., Yan H.,
750 Caroll S., Pace M. N., Nyman J., Luo J., Gentile M. E., Fields M. W., Hickey R.
751 F., Gu B., Watson D., Cirpka O. A., Zhou J., Fendorf S., Kitanidis P. K., Jardine P.
752 M., and Criddle C. S. (2006b) Pilot-Scale in Situ Bioremedation of Uranium in a
753 Highly Contaminated Aquifer. 2. Reduction of U(VI) and Geochemical Control of
754 U(VI) Bioavailability. *Environ. Sci. Technol.* 40(12), 3986-3995.
755 Zhang G., Kim J., Dong H., and Andre J. S. (2007a) Microbial effects in promoting the
756 smectite to illite reaction: Role of organic matter intercalated in the interlayer.
757 *American Mineralogist* 92, 1401-1410.

758 Zhang G., Dong H., Kim J., and Eberl D. D. (2007b) Microbial Reduction of Structural
759 Fe^{3+} in Nontronite by a Thermophilic Bacterium and its Roles in Promoting the
760 Smectite to Illite Reaction. *American Mineralogist* 92, 1411-1419.
761 Zhou P., and Gu B. H. (2005) Extraction of oxidized and reduced forms of uranium from
762 contaminated soils: Effects of carbonate concentration and pH. *Environmental*
763 *Science & Technology* 39(12), 4435-4440.
764

765 **Table 1.** Standard state reduction potentials (E^0) for iron oxides, nontronite, uranium,

766 technetium, and experimental components.

Redox couple (eq #)	E^0 (V)
Ferrihydrite, $Fe(OH)_3$ $Fe(OH)_{3(s)} + 2H^+_{(aq)} + e^- + HCO^-_{3(aq)} \rightarrow FeCO_{3(s)} + 3H_2O_{(l)}$	0.971 [a]
Goethite, α-$FeOOH_{(s)}$ α-$FeOOH_{(s)} + 2H^+_{(aq)} + e^- + HCO_{3(aq)} \rightarrow FeCO_{3(s)} + 2H_2O_{(l)}$	0.848 [a]
Pertechnetate, TcO_4^- $TcO_4^-{}_{(aq)} + 4H^+_{(aq)} + 3e^- \rightarrow TcO_2 \cdot nH_2O_{(s)} + (2\text{-}n)H_2O_{(l)}$	0.748 [b]
Nontronite SWa-1 (Eq. 2) $mFe^{3+}_{(s)} + w_0Na^+_{(s)} + n_i(OH^-)_{(s)} + me^- + pNa^+_{(aq)} + n_iH^+_{(aq)} \rightarrow$ $mFe^{2+}_{(s)} + wNa^+_{(s)} + n_iH_2O_{(l)}$	0.70 [c]
Uranyl carbonate, $UO_2(CO_3)_3^{4-}$ $0.5UO_2(CO_3)^{4-}_{3(aq)} + 1.5H^+_{(aq)} + e^- \rightarrow 0.5UO_{2(s)} + 1.5HCO^-_{3(aq)}$	0.687 [a]
Ca-U(VI)-CO_3 complex, $CaUO_2(CO_3)_3^{2-}$ $0.5CaUO_2(CO_3)_3^{2-}{}_{(aq)} + 1.5H^+_{(aq)} + e^- \rightarrow 0.5UO_{2(s)} + 1.5HCO^-_{3(aq)} + 0.5Ca^{2+}$	0.576 [d]
Nontronite NAu-2 (Eq. 1) $Na_{.71}Mg_{.05}Fe_{3.83}Al_{.5}Si_{7.55}O_{20}(OH)_{4(s)}$ (NAu-2) $+ 3.83e^- + 11.8H^+_{(aq)} \rightarrow$ $0.71Na^+_{(aq)} + 0.05Mg^{2+}_{(aq)} + 3.83Fe^{2+}_{(aq)} + 0.5Al(OH)_4^-{}_{(aq)} + 7.55SiO_{2(aq)} + 6.9H_2O_{(l)}$	0.60 [e]
Ca_2-U(VI)-CO_3 complex, $Ca_2UO_2(CO_3)_{3(aq)}$ $0.5Ca_2UO_2(CO_3)_3^{2-}{}_{(aq)} + 1.5H^+_{(aq)} + e^- \rightarrow 0.5UO_{2(s)} + 1.5HCO^-_{3(aq)} + Ca^{2+}$	0.424 [c]
Anthraquinone-2,6-disulfonate, AQDS $0.5AQDS_{(aq)} + H^+_{(aq)} + e^-_{(aq)} \rightarrow 0.5AH_2DS_{(aq)}$	0.230 [f]
Acetate/lactate, $CH_3COO^-/C_2H_5COO^-$ $0.25CH_3COO^-_{(aq)} + 0.25HCO^-_{3(aq)} + 1.25H^+_{(aq)} + e^-_{(aq)} \rightarrow$ $0.25C_2H_5COO^-_{(aq)} + 0.5H_2O_{(l)}$	0.121 [f]

767 [a] Fredrickson et al. (2002) *Geochim. Cosmochim. Acta*. 66, 3247–3262.
768 [b] Peretyazhko et al. (2008) *Geochim. Cosmochim. Acta*. 72, 1521–1539.
769 [c] Favre et al. (2006) *Clays and Clay Minerals*. 54, 466-472.
770 [d] Brooks et al. (2003). *Environ. Sci. Technol*. 37, 1850-1858.
771 [e] Jaisi et al. (2007b) *Geochim. Cosmochim. Acta*. 71, 1145-1158.
772 [f] Fredrickson et al. (2000) *Geochim. Cosmochim. Acta*. 64, 3085–3098.
773

774 **Table 2.** Average valence states of Fe and U within uranium-nontronite samples as
775 determined by wet chemical methods and linear combination fitting of the XANES
776 spectra. Sample names correspond to XANES spectra presented in Figure 9.

Sample name/description	**% Fe(II) in Nontronite**		**% U(IV) in precipitates**	
	0.5 N HCl extraction	**Fe-XANES**	**1 M $NaHCO_3$ extraction**	**U-XANES**
NUC 5 g L^{-1} Nontronite NAu-2 + 1 mM Uranyl(VI) acetate + 0 MR-1 (abiotic control) incubated for 52 days	0.38 ± 3.0	0 ± 10	-3.5 ± 4.1	0 ± 10
NUR 5 g L^{-1} Nontronite NAu-2 + 1 mM Uranyl(VI) acetate + $1*10^8$ cell mL^{-1} MR-1 incubated for 52 days	28.3 ± 1.6	38 ± 10	82.7 ± 2.7	90 ± 10
NUO NUR sample reacted with dissolved oxygen for 20 hrs	13.3 ± 0.2	18 ± 10	30.6 ± 0.8	20 ± 10

777

778 **Table 3.** Concentrations of select dissolved metals measured before and after
779 bioreduction of nontronite by *Shewanella putrefaciens* CN32 (Zhang et al., 2007a).
780 Experiments conducted with 5.0 g L^{-1} nontronite NAu-2 and 5.0 mM sodium lactate in
781 anoxic 30 mM $NaHCO_3$ (pH 6.8; 80:20% N_2:CO_2 atm) incubated with $0.5*10^8$ cell mL^{-1}
782 CN32 for 23 days.

Reaction time (days)	0	23
Ca (mM) [a]	0.06	0.27
Mg (mM)	0.68	1.16
Si (mM)	0.83	0.79
Al (mM)	<0.001	<0.001
Fe_T (mM)	0.021	0.036
0.5 N HCl-extractable Fe(II) (mM) reduction extent (% Fe(II)/Fe_T)	0.10 0.5%	4.3 20.5%
pH	6.8	6.8

783 [a] Mg, Ca, Si, Al and Fe_T measured by ICP-MS where samples were first filtered (0.2-μm)
784 and acidified with conc. HNO_3. Zhang et al. (2007a) *American Mineralogist*. 92, 1401-
785 1410.
786

787 **Table 4.** Comparison of uranyl(VI) sorption to nontronite NAu-2 (current study) with

788 other smectites.

Reference	Solid-phase	Solution chemistry	Sorption characteristics
Ames et al., (1983)	Nontronite NG-1 CEC = 95 meq/100g SA = 861 m^2/g	10 mM $NaHCO_3$ pH 8.5	Γ_{max} =1.21*10^{-7} mole/m^2 K_d = 4.1 ml/g
Ames et al., (1983)	Nontronite NG-1 CEC = 95 meq/100g SA = 861 m^2/g	10 mM NaCl pH 7.0	Γ_{max} =6.55*10^{-7} mole/m^2 K_d = 300 ml/g
Ames et al., (1983)	Montmorillonite CEC = 120 meq/100g SA = 747 m^2/g	10 mM $NaHCO_3$ pH 8.5	Γ_{max} =8.99*10^{-8} mole/m^2 K_d = 1.8 ml/g
Ames et al., (1983)	Montmorillonite CEC = 120 meq/100g SA = 747 m^2/g	10 mM NaCl pH 7.0	Γ_{max} =1.18*10^{-6} mole/m^2 K_d = 542 ml/g
Ames et al., (1982)	Smectite CEC = 4.84meq/100g SA = 31.2 m^2/g	Hanford groundwater pH 7.7	Γ_{max} =3.34*10^{-3} mole/m^2 K_d = 12 – 127 ml/g
Catalano and Brown (2005)	Montmorillonite SWy-2 CEC = 85meq/100g SA = 31.8 m^2/g	100 mM $NaNO_3$ pH 7.1	Γ_{max} =9.57*10^{-3} mole/m^2 K_d = 8.2 ml/g
Current study	Nontronite NAu-2 CEC=69.7 meq/100g SA = 42 m^2/g	30 mM $NaHCO_3$ pH 7.0	Γ_{max} =1.73*10^{-3} mole/m^2 K_d = 64.9 ml/g

789 Ames et al. (1983) *Chemical Geology*. 35, 205-225.

790 Ames et al. (1982) *Clays and Clay Minerals*. 31, 321-334.

791 Catalano and Brown. (2005) *Geochim. Cosmochim. Acta.* 69, 2995-3005.
792

FIGURE CAPTIONS

Figure 1. Uranyl(VI) speciation as a function of U(VI) concentration in 30 mM $NaHCO_3$ in equilibrium with an 80:20 % N_2:CO_2 atm at pH 6.8 with (a) 0 mM Ca and 0 mM Mg (no nontronite); (b) 0.06 mM Ca and 0.68 mM Mg (with nontronite before bioreduction); and (c) 0.27 mM Ca and 1.16 mM Mg (after bioreduction of nontronite).

Figure 2. (a) U(VI) sorption edge on nontronite NAu-2 (3.0 g L^{-1}) as a function of pH in 0.001 M, 0.01 M, 0.1 M and 1 M $NaNO_3$ background electrolytes ([Total U(VI)] = 0.01 mM). Symbols represent means of duplicate measurements. (b) U(VI) sorption isotherm on nontronite NAu-2 (5.0 g L^{-1}) in anoxic 30 mM $NaHCO_3$, pH 6.8. Symbols represent means of duplicate measurements and error bars represent 1 standard deviation.

Figure 3. Biological reduction of U(VI) and nontronite NAu-2 Fe(III) by *S. oneidensis* MR-1 ($0.5*10^8$ cells mL^{-1}) in the presence or absence of AQDS (0.1 mM). Experiments were conducted with 1.0 mM U(VI), 5.0 g L^{-1} nontronite NAu-2 and 5.0 mM lactate in 30 mM $NaHCO_3$, pH 6.8. (a) Aqueous U(VI), (b) 0.5 N HCl-extractable Fe(II), and (c) Surface-adsorbed Fe(II). Symbols represent means of triplicate measurements and error bars represent 1 standard deviation.

Figure 4. Biological reduction of U(VI) in the presence of variable concentrations of nontronite NAu-2 by *S. oneidensis* MR-1 ($1.0*10^8$ cells mL^{-1}). Experiments were conducted with 0.7 – 0.8 mM U(VI) and 5.0 mM lactate in 30 mM $NaHCO_3$, pH 6.8. (a) Time-dependent consumption of soluble U(VI), and (b) final extent of U(VI) and Fe(III)

816 (0.5 N HCl-extractable Fe(II)) reduction after 52 d. Symbols represent means of
817 duplicate measurements and error bars represent 1 standard deviation.
818
819 **Figure 5.** Biological reduction of nontronite NAu-2 in the presence of variable
820 concentrations of U(VI) by *S. oneidensis* MR-1 ($1.0*10^8$ cells mL^{-1}). Experiments were
821 conducted with 5.0 g L^{-1} nontronite NAu-2 and 5.0 mM lactate in 30 mM $NaHCO_3$, pH
822 6.8. (a) Time-dependent production of 0.5 N HCl-extractable Fe(II), and (b) final extent
823 of U(VI) and Fe(III) (0.5 N HCl-extractable Fe(II)) reduction after 52 d. Inset in (b)
824 shows final extent at lowest U(VI) concentrations tested. Symbols represent means of
825 duplicate measurements and error bars represent 1 standard deviation.
826
827 **Figure 6.** Abiotic oxidation of biogenic uraninite (0.14 mM) by unaltered nontronite
828 NAu-2 (5 g L^{-1}, 99.4% Fe(III)) in 30 mM $NaHCO_3$, pH 6.8. Symbols represent means of
829 duplicate measurements and error bars represent 1 standard deviation.
830
831 **Figure 7.** Abiotic reduction of 0.23 mM U(VI) by chemically reduced nontronite NAu-2
832 (2.5 g L^{-1}, 27% Fe(II)) in 30 mM $NaHCO_3$, pH 6.8.
833
834 **Figure 8.** (a) Scanning electron micrographs of unstained *Shewanella oneidensis* MR-1
835 cells and uraninite produced in the absence of nontronite NAu-2. Inset is SEM-EDS
836 spectrum of uraninite showing typical elemental composition (Au peak from Au coating).
837 (b) Secondary electron image of abiotic control (no cells) containing nontronite NAu-2
838 and U(VI). Inset is SEM-EDS spectrum showing typical elemental composition. (c)

839 Secondary electron image of uraninite produced in the presence of nontronite NAu-2. (d)
840 Secondary electron image of bioreduced nontronite NAu-2 in the absence of uranium.
841
842 **Figure 9.** (A) Fe K edge normalized XANES spectra offset vertically by 1.0, and (B)
843 overlaid. (C) U L_{III}-edge normalized XANES spectra offset vertically by 0.8, and (D)
844 overlaid. The measured spectra (symbols) from the samples are over-plotted by linear
845 combination fitting of the XANES spectra (solid lines). The reduced standards (Fe(II)
846 and U(IV)) are shown as blue lines while the oxidized standards (Fe(III) and U(VI)) are
847 shown as black lines. The samples shown from bottom to top in panels (A) and (C) are:
848 NUC – 5 g L^{-1} nontronite NAu-2, 1 mM uranyl(VI) acetate, and no cells; NUR – 5 g L^{-1}
849 nontronite NAu-2, 1 mM uranyl(VI) acetate, $1*10^8$ cell mL^{-1} MR-1 and incubated for 52
850 days; NUO – the NUR sample reacted with dissolved oxygen for 20 hrs.
851
852 **Figure 10.** Conceptualization of operative reactions in experiments conducted with
853 nontronite NAu-2, uranium and dissimilatory metal-reducing bacteria (DMRB).
854

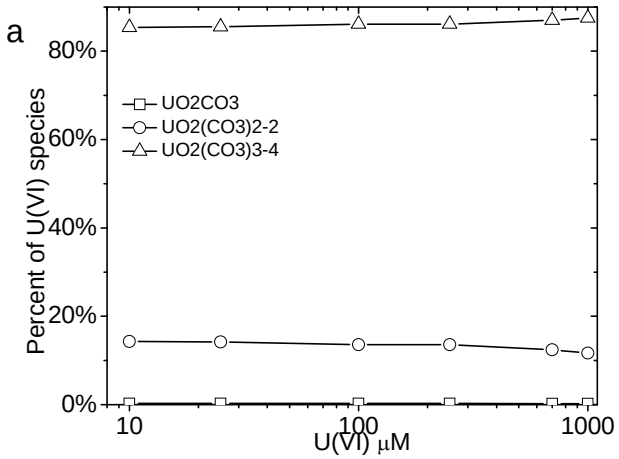

855

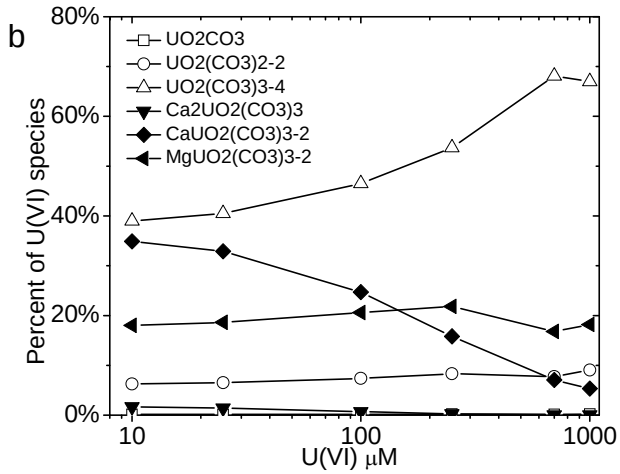

856

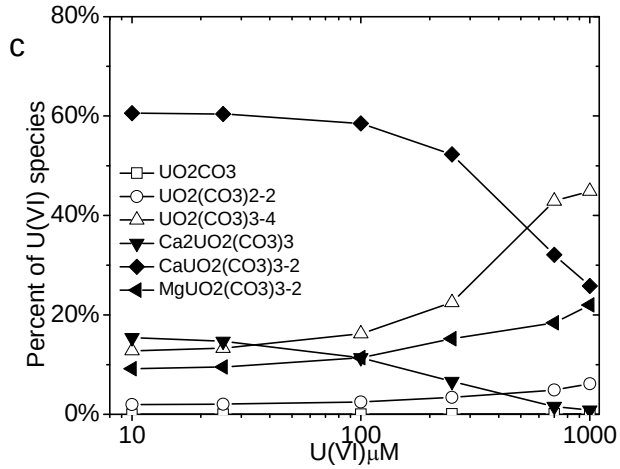

857
858 Figure 1
859

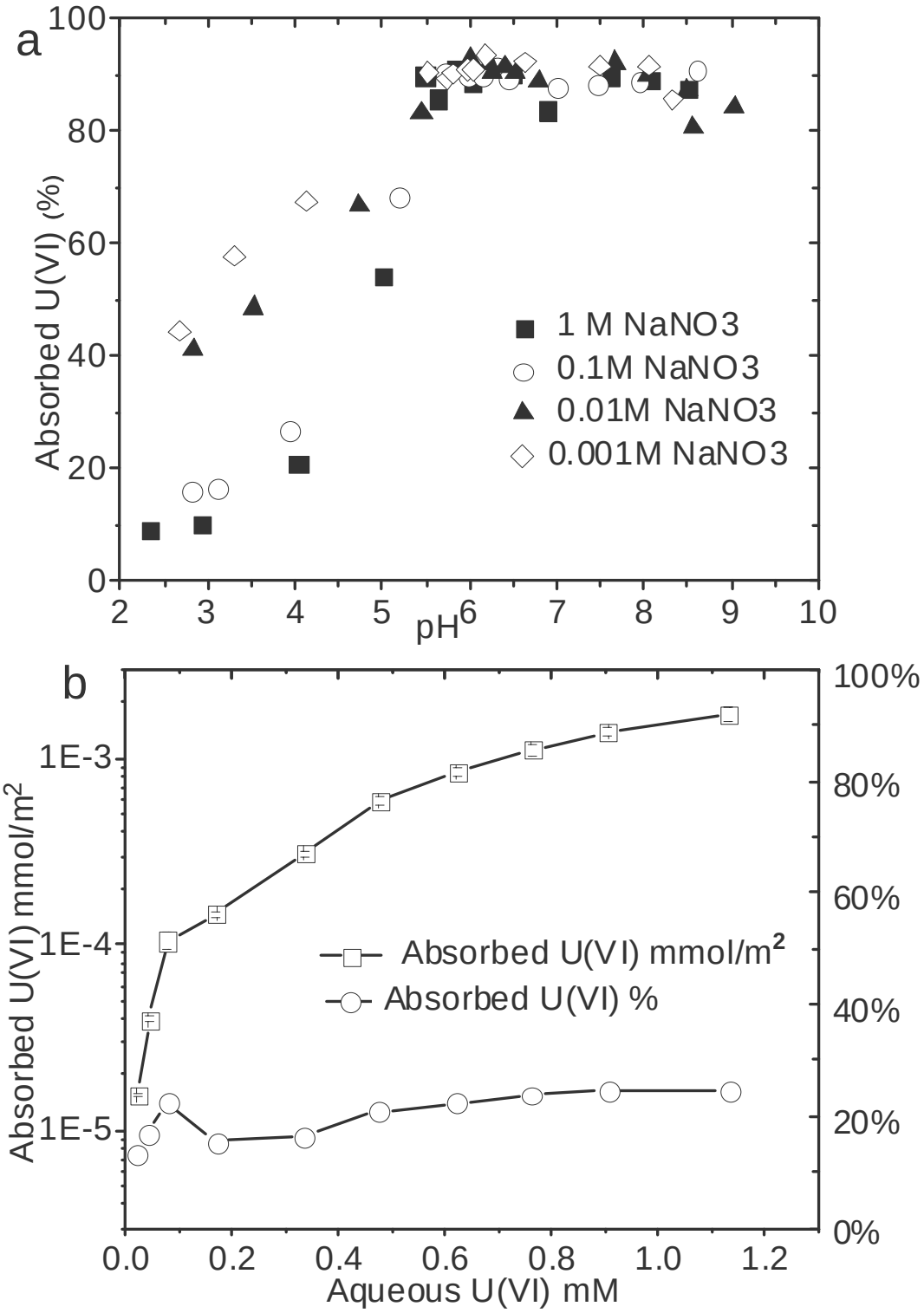
a
Absorbed U(VI) (%)
pH
1 M NaNO3
0.1M NaNO3
0.01M NaNO3
0.001M NaNO3
b
Absorbed U(VI) mmol/m²
Absorbed U(VI) %
Aqueous U(VI) mM

Figure 2

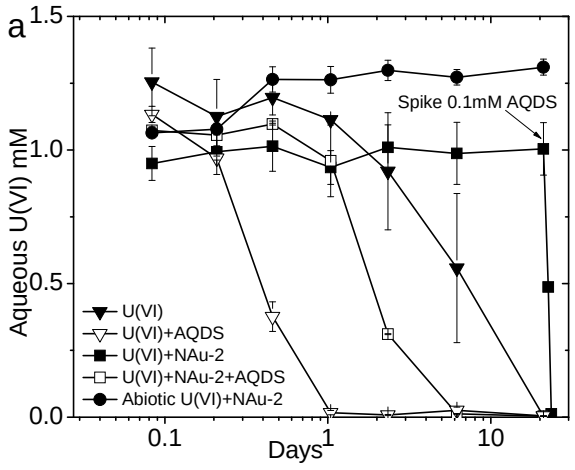

863

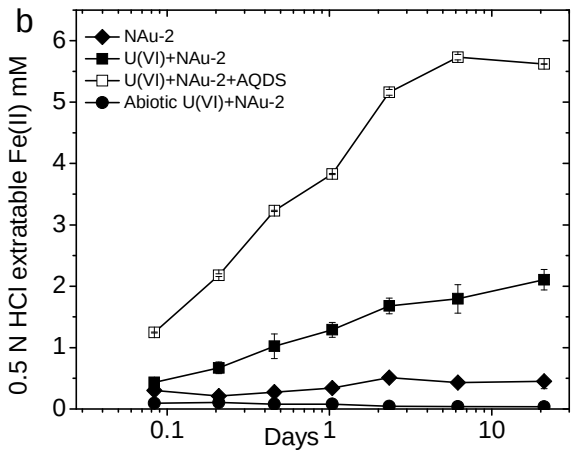

864

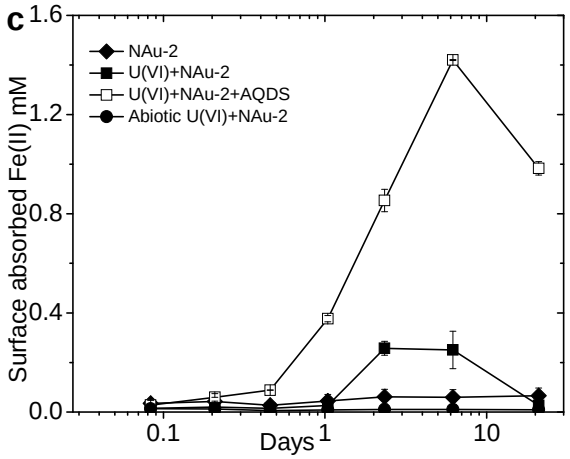

865
866 Figure 3

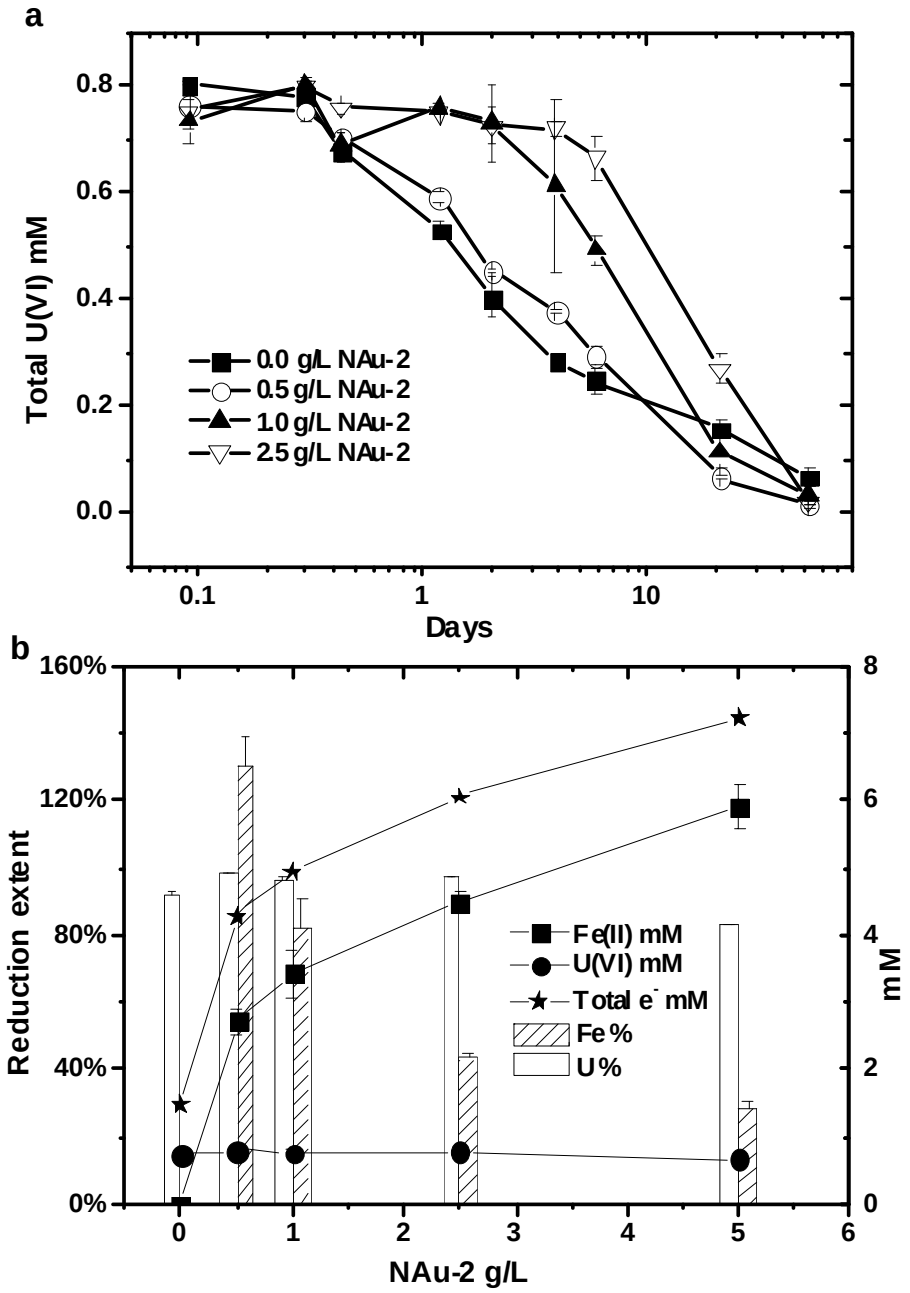

867
868 Figure 4
869

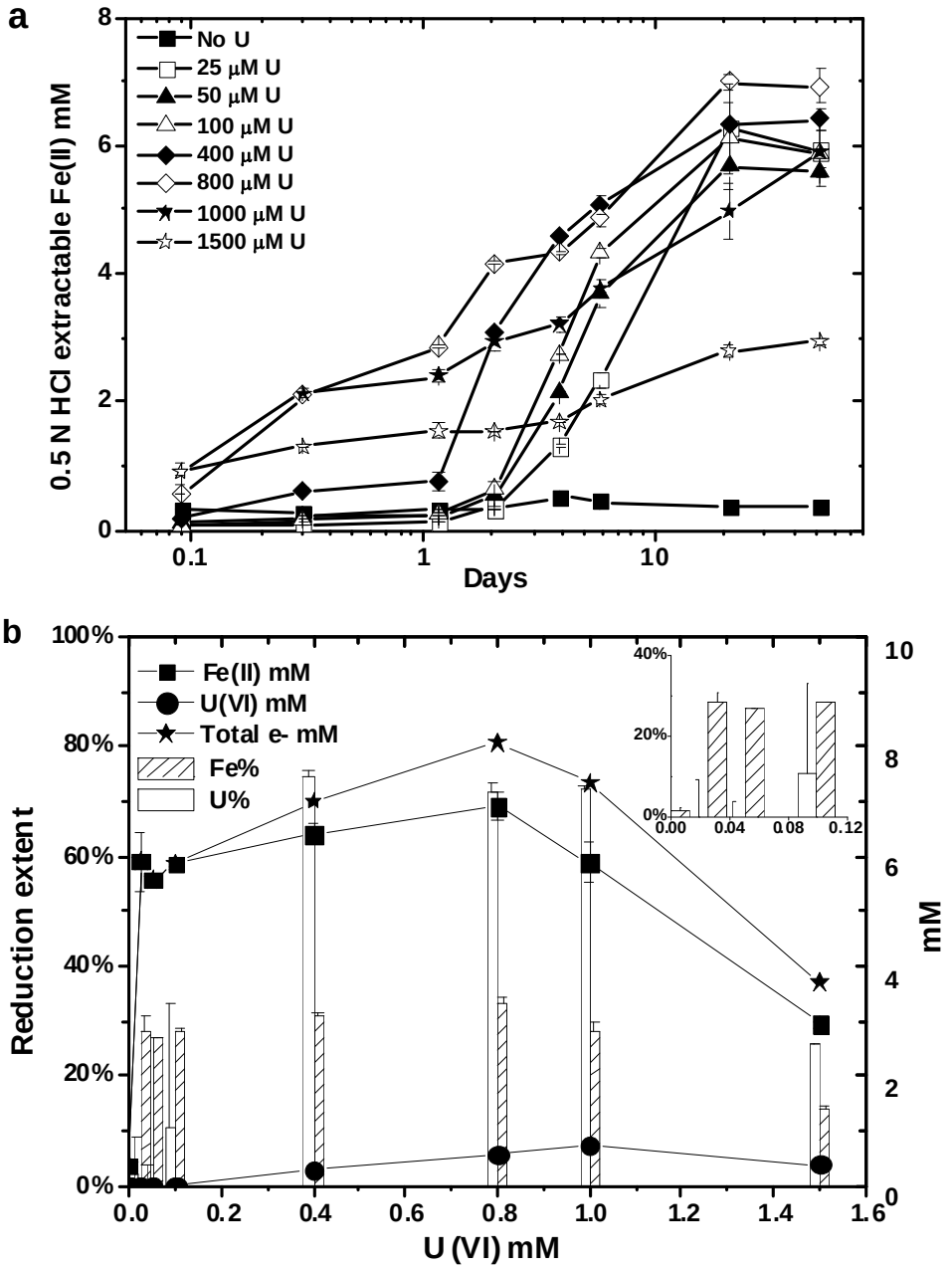

870
871 Figure 5
872

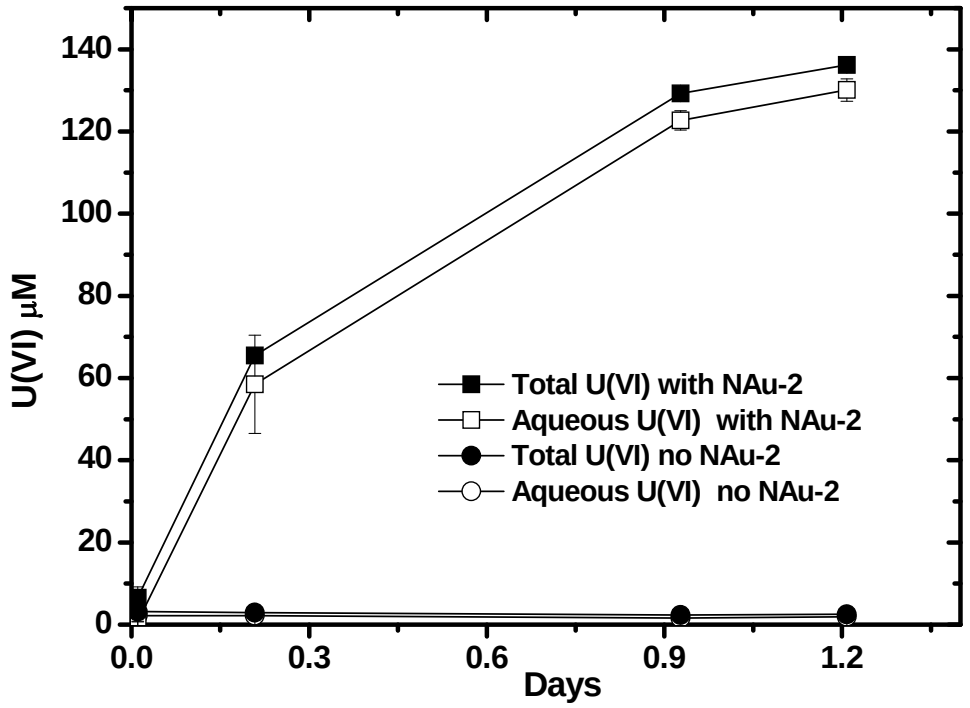

873
874 Figure 6

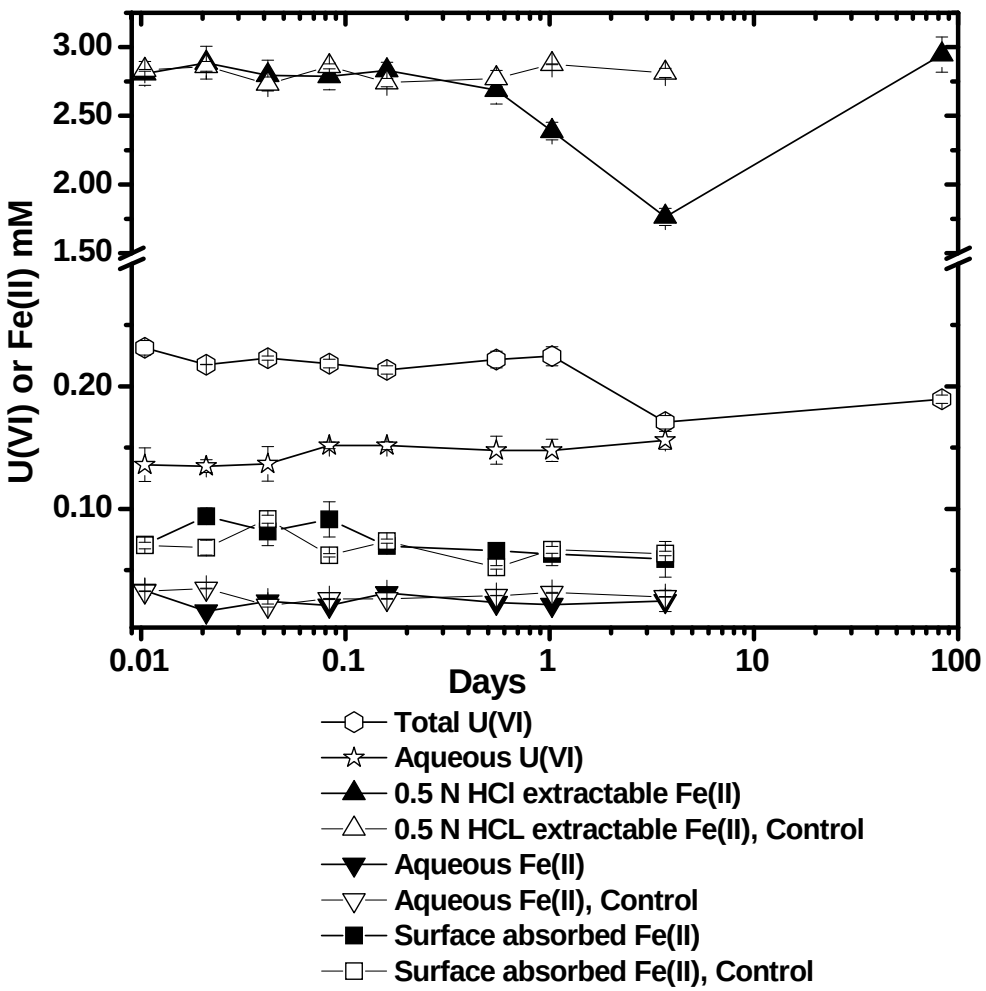

875
876 Figure 7
877

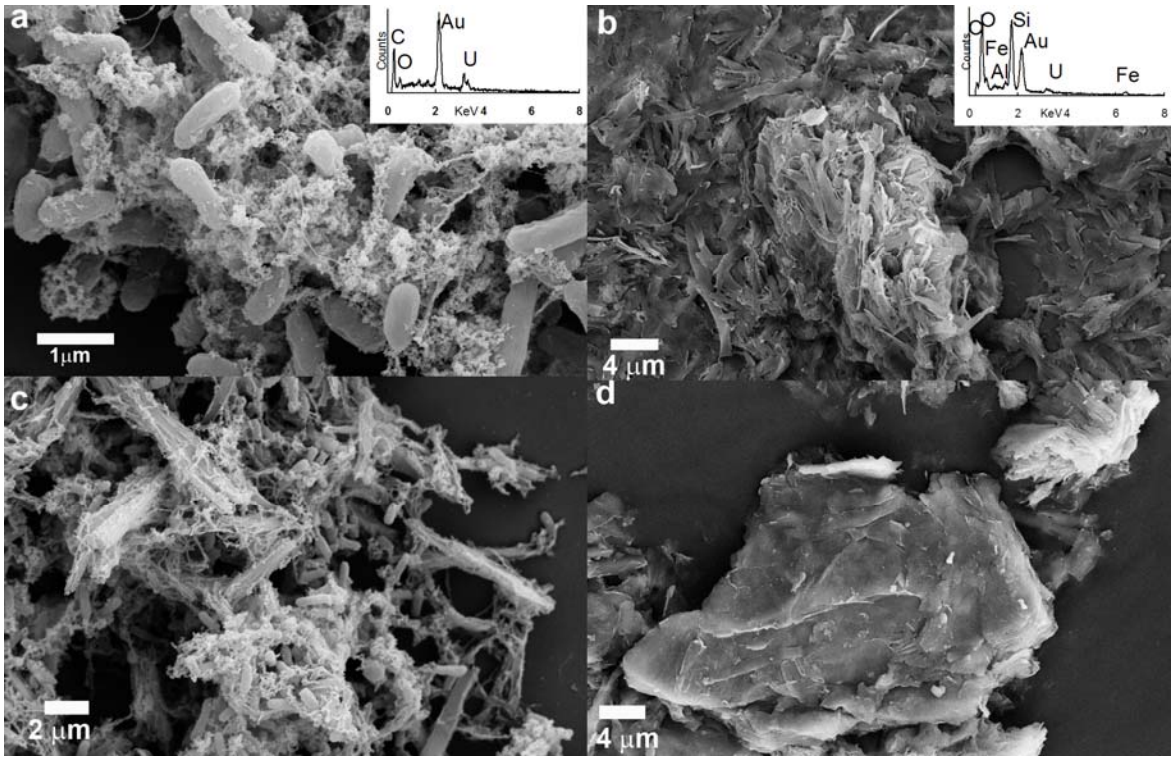
a
Counts
C
O
Au
U
0 2 KeV 4 6 8
1μm
b
Counts
O
Fe
Al
Si
Au
U
Fe
0 2 KeV 4 6 8
4 μm
c
2 μm
d
4 μm

Figure 8

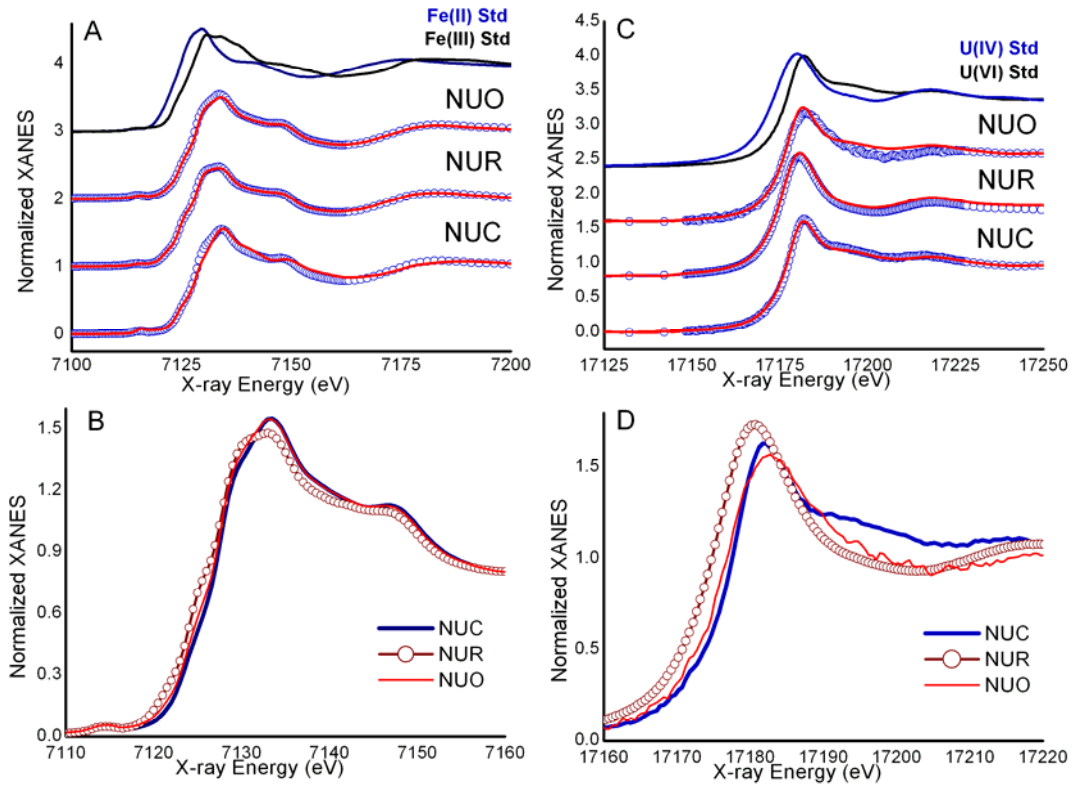

882
883 Figure 9
884

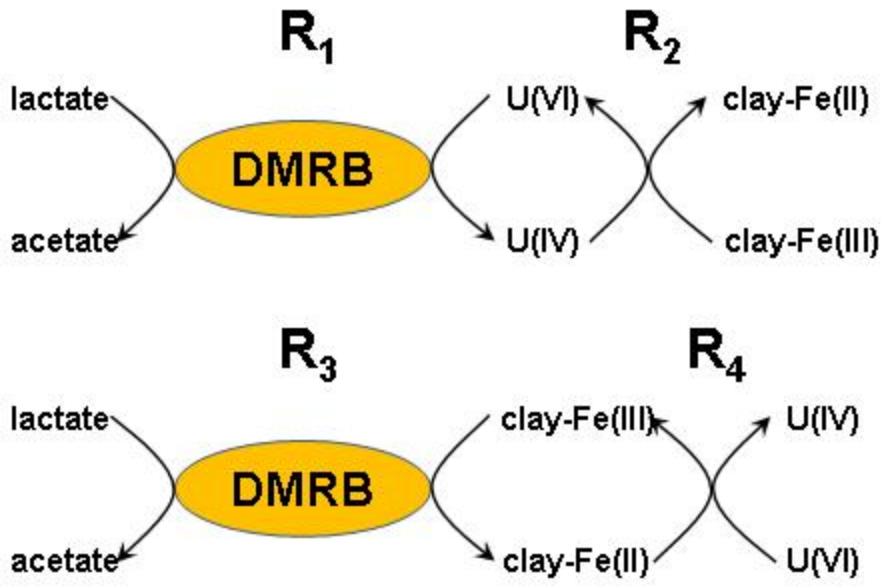

885
886 Figure 10
887

Electronic Annexes EA-1 and EA-2

Microbial reduction of iron(III)-rich nontronite and uranium(VI)

Gengxin Zhang[1], John M. Senko[1], Shelly D. Kelly[2], Hui Tan[1], Kenneth M. Kemner[2] and William D. Burgos[1*]

[1]Department of Civil and Environmental Engineering, The Pennsylvania State University, University Park, PA, [2]Biosciences Division, Argonne National Laboratory, Argonne, IL.

EA-1 U(VI) speciation modeling.

EA-2 X-ray diffraction of nontronite and uraninite.

EA-1 U(VI) speciation modeling.

Table EA-1. Uranium(VI) aqueous and solid phase reactions and thermodynamic stability constants used with PHREEQC for U speciation modeling.

Reaction	log K
$UO_2^{2+} + H_2O = UO_2OH^+ + H^+$	-5.78 [a]
$UO_2^{2+} + 2H_2O = UO_2(OH)_2(aq) + 2H^+$	-12.15 [b]
$UO_2^{2+} + 3H_2O = UO_2(OH)_3^- + 3H^+$	-19.2 [b]
$UO_2^{2+} + 4H_2O = UO_2(OH)_4^{2-} + 4H^+$	-32.4 [b]
$2UO_2^{2+} + 3H_2O = (UO_2)_2(OH)_3^+ + 3H^+$	-2.70 [b]
$2UO_2^{2+} + 2H_2O = (UO_2)_2(OH)_2^{2+} + 2H^+$	-5.62 [a,b]
$3UO_2^{2+} + 4H_2O = (UO_2)_3(OH)_4^{2+} + 4H^+$	-11.90 [b]
$3UO_2^{2+} + 5H_2O = (UO_2)_3(OH)_5^+ + 5H^+$	-15.63 [a]
$3UO_2^{2+} + 7H_2O = (UO_2)_3(OH)_7^- + 7H^+$	-31.0 [b]
$UO_2^{2+} + CO_3^{2-} = UO_2(CO_3)^0$	+10.06 [a]
$UO_2^{2+} + 2CO_3^{2-} = UO_2(CO_3)_2^{2-}$	+16.98 [a]
$UO_2^{2+} + 3CO_3^{2-} = UO_2(CO_3)_3^{4-}$	+21.40 [a]
$2UO_2^{2+} + CO_3^{2-} + 3H_2O = (UO_2)_2CO_3(OH)_3^- + 3H^+$	-0.94 [b]
$UO_2^{2+} + 3CO_3^{2-} + Ca^{2+} = CaUO_2(CO_3)_3^{2-}$	27.18 [c]
$UO_2^{2+} + 3CO_3^{2-} + 2Ca^{2+} = Ca_2UO_2(CO_3)_3^0$	30.7 [c]
$UO_2^{2+} + 3CO_3^{2-} + Mg^{2+} = MgUO_2(CO_3)_3^{2-}$	25.8[b]
$UO_2^{2+} + NO_3^- = UO_2NO^+$	0.3 [b]
$UO_2^{2+} + 3H_2O = UO_2(OH)_2{\cdot}H_2O(\text{schoepite}) + 2H^+$	-5.39 [a]

[a] Langmuir, D. (1978) Uranium solution-mineral equilibria at low temperatures with applications to sedimentary ore deposits. *Geochim. Cosmochim. Acta* **42**, 547–569.

[b] Guillaumont, R., T. Fanghänel, J. Fuger, I. Grenthe, V. Neck, D.A. Palmer and M.H. Rand. (2003) Update on the Chemical Thermodynamics of Uranium, Neptunium, Plutonium, Americium and Technetium. Elsevier, Amsterdam.

[c] Dong, W., and S.C. Brooks. (2006) Determination of the Formation Constants of Ternary Complexes of Uranyl and Carbonate with Alkaline Earth Metals (Mg^{2+}, Ca^{2+}, Sr^{2+}, and Ba^{2+}) Using Anion Exchange Method. *Environ. Sci. Technol.* **40**, 4689-4695.

[d] Dong, W., and S.C. Brooks. (2008) Formation of Aqueous $MgUO_2(CO_3)_3^{2-}$ Complex and Uranium Anion Exchange Mechanism onto an Exchange Resin. *Environ. Sci. Technol.* **42**, 1979-1983.

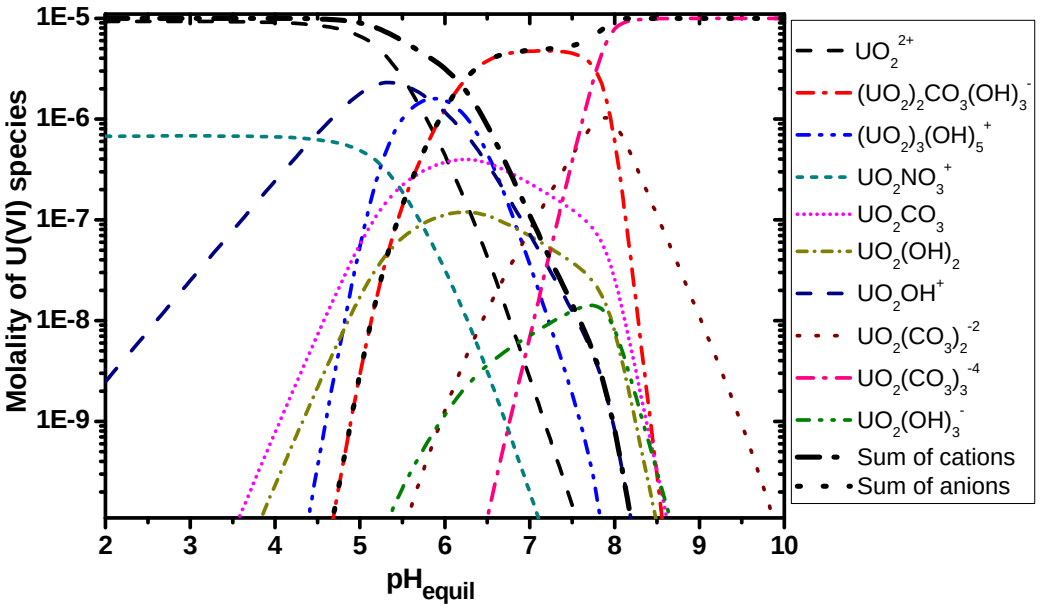

915

916 **Figure EA-1.** Uranyl(VI) speciation as a function of pH in the presumed solution

917 chemistry for one of the sorption edge experiments – 10 μM uranyl acetate, 0.01 M

918 $NaNO_3$ in equilibrium with air ($P_{CO2} = 10^{-3.46}$ bar), Ca and Mg both assumed equal 0 mM

919 for all pH values.

920

EA-2 X-ray diffraction of nontronite and uraninite.

Samples for X-ray diffraction (XRD) were washed with deoxygenated water and air dried in an anoxic glovebox and prepared in ambient condition for XRD measurements. Samples were examined using a Rigaku Geigerflex microdiffractometer equipped with a graphite monochromater and a cylindrical image plate area detector. A Mo tube was used as the X-ray source and a 0.3 mm collimator was used to ensure parallel X-ray beams. Samples were mounted on a flat quartz zero-background holder using petroleum-based grease. During exposure to the X-ray beam, the sample was oscillated between 2 to 10° omega angle and -30 to +30° phi angle simultaneously to minimize the effects of sample heterogeneity and preferred orientation.

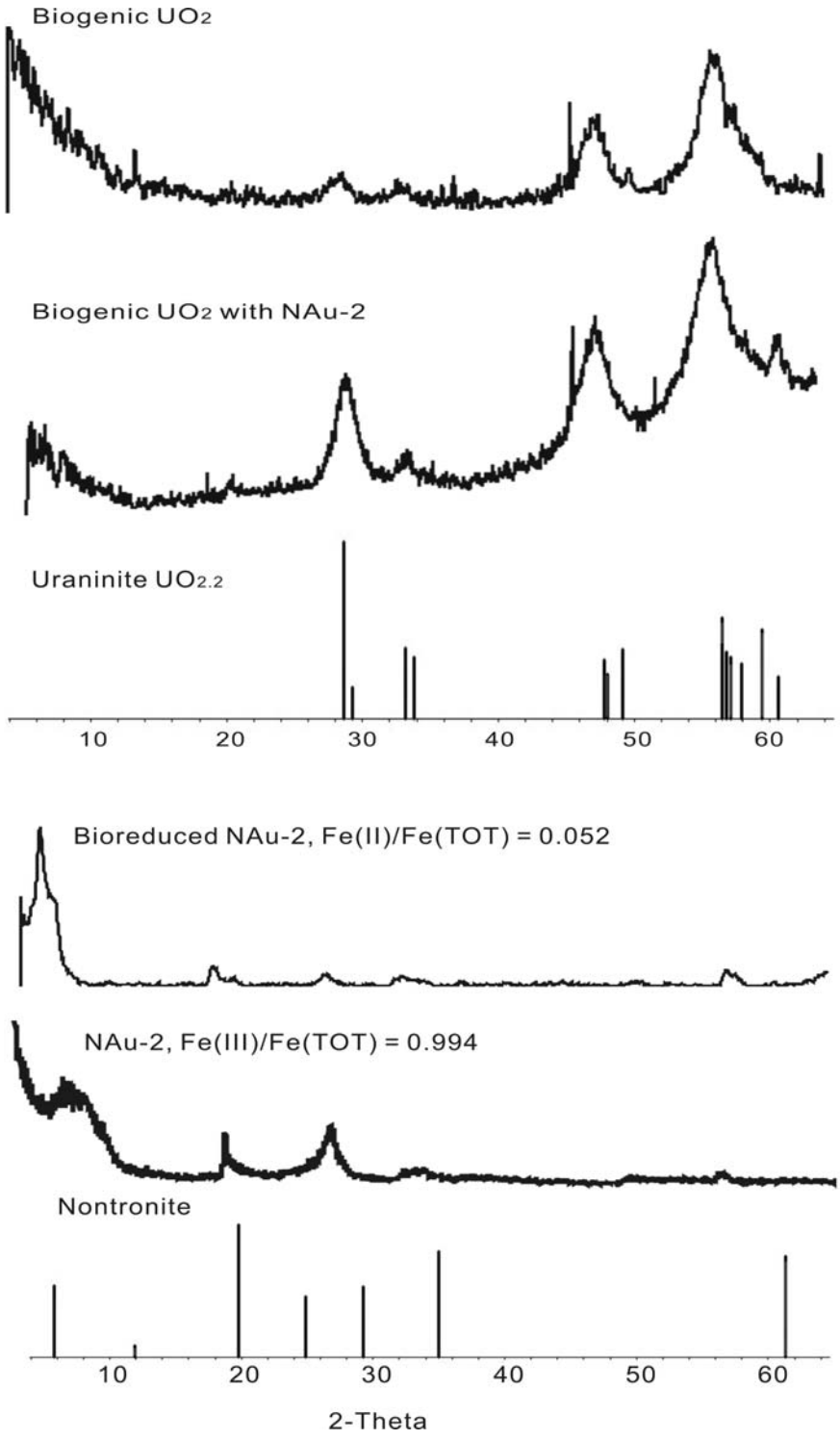

931

932 **Figure EA-2.** X-ray diffraction patterns from biogenic uraninite, biogenic uraninite produced in

933 the presence of nontronite NAu-2, bioreduced NAu-2 in the absence of U(VI), and the unaltered

934 nontronite NAu-2.